tissue-engineered cartilage tissues cultured for various periods (up to 12 weeks) were used as samples. By comparing the results of biochemical analyses and biomechanical studies, we confirmed the photoacoustic signal as a good indicator for evaluating extracellular matrix formation in order to determine the characteristics of tissue-engineered cartilage [29–38]. We also developed a method for extracellular matrix characterization using TR-LIFS, which enabled simultaneous measurements with mechanical properties using the photoacoustic method [39–41].

We propose the application of these unique measurements and evaluation methodologies [29–41], which we have developed in vitro to non-invasively assess regenerating cartilage (tissue-engineered cartilage) and to diagnose cartilage degeneration. When used in clinical settings, our laser measurement method requires arthroscopy, but the amount of information obtained is greater than that provided by other devices (Table 1). This method may thus be a useful assessment technique in clinical studies that closely assess cartilage.

## MATERIALS AND METHODS

Scattering, reflection, and increase in temperature attributable to absorption and the production of fluorescence and acoustic waves are regarded as the main effects when light or laser beams irradiate living organs to be measured (Fig. 1) [42]. A non-invasive and selective diagnostic device that uses optics via a fiber optic cable has recently attracted attention. This device is based on a technology that takes advantage of interactions between optics and living organs. Use of these interactions enables simultaneous collection of not only morphological information, but also various physiological and biochemical data, so the potential for use as a diagnostic device is greater than that of techniques based on a single type of information, such as ultrasonic waves. Bioinstrumentation and imaging with a laser beam, which have recently attracted attention, show features that facilitate the application of this technology to medical fields. We have focused on the interactions between living organs and optics (particularly photoacoustic waves and fluorescence), measured a variety of parameters related to these interactions when induced by the same laser, and developed a system that allows the simultaneous evaluation of the mechanical characteristics and properties of tissue (Fig. 2) [32,33,38].

### Evaluation of Mechanical Characteristics Using a Photoacoustic Method

Tissue viscoelasticity affects the propagation and attenuation of the stress waves induced by pulsed laser irradiation [29]. The relaxation time of the stress wave, calculated as the time in which the amplitude of the stress wave decreases by a factor of $1/e$, gives the intrinsic relaxation parameters ($\eta/G$) of the tissue, where $\eta$ is the viscosity and $G$ is the elasticity. We have proposed a basic principle whereby the mechanical characteristics of the tissue can be measured using photoacoustic parameters. In this measurement technique, the relaxation time of the

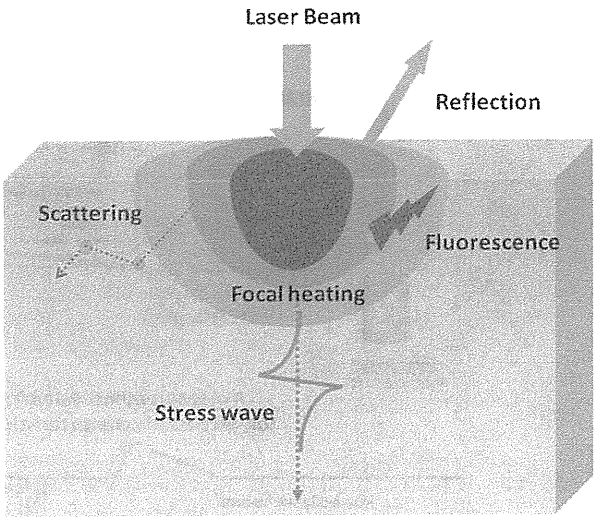


Fig. 1. Mutual interaction between light and a living body. The scattering, reflection, and increase in temperature attributable to absorption and the production of fluorescence and acoustic waves are regarded as the main effects when light or laser beams irradiate living organs to be measured. The figure was cited and modified from Bioengineering: Principles, Methodologies, and Applications ISBN: 978-1-60741-762-0 Authors: M. Sato et al., Editors: A. Garcia et al., pp. 179–190, 2010 Nova Science Publishers, Inc. Chapter 7.

stress that acts on a linear viscoelastic object (consisting of a spring and a dashpot) is related to the viscoelastic parameters of the object, and to the damping time of the stress waves generated by irradiation with a nanosecond pulse laser. Relaxation time is theoretically related to the viscoelastic ratio [42]. The relaxation time ($\tau$) is calculated using the Levenberg–Marquardt algorithm, a nonlinear least-squares method, as follows. When the stress wave intensity is attenuated only by its reflection at the boundaries and its relaxation during its transmission through viscoelastic materials, then the time course of the stress wave intensity is expressed by the following equation [34]:

$$I_\delta = I_0 \times R \times \exp\left(\frac{-t_\delta}{\tau}\right),$$

where $I_0$ is the intensity of the stress wave at $t = 0$, $R$ is the product of reflectivity (the product of the internal reflectivity at the interface at both ends of the sample), $t_\delta$ is the time after laser irradiation, and $\tau$ is the damping time of the stress wave and corresponds to the viscoelastic ratio.

As the optimum wavelength of the laser beam was unknown at the beginning of this study, we used an optical parametric oscillator (Spectra-Physics, Tokyo, Japan) with the original probe (Fig. 3) and set the oscillation wavelength within the range of 250–355 nm, with collagen and protein as the optical absorbers.

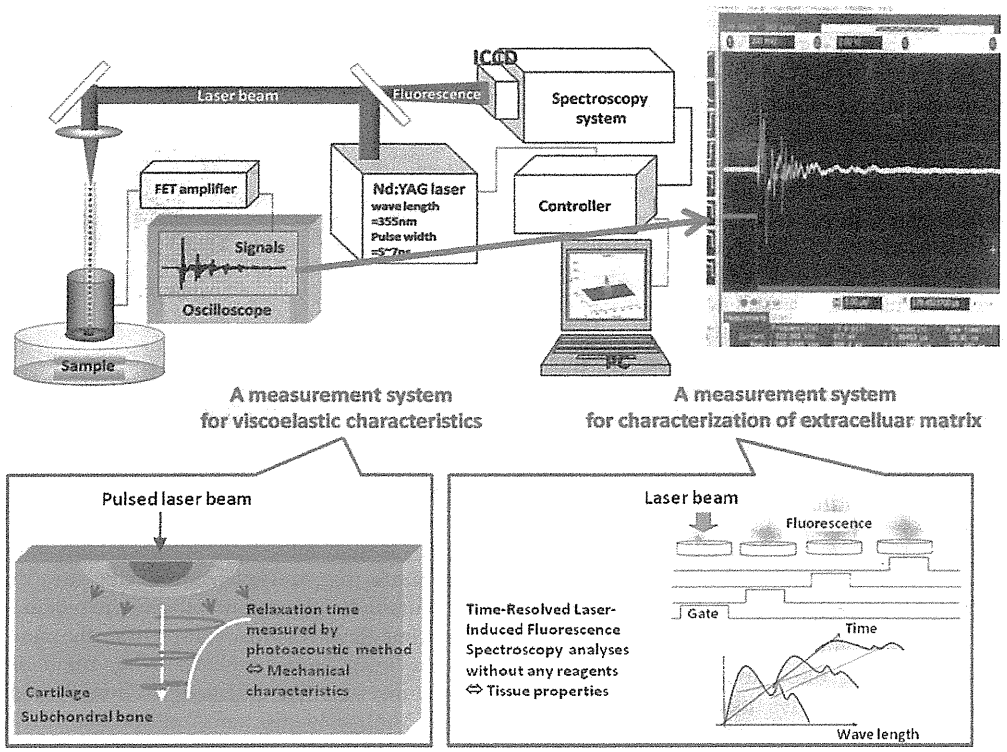


Fig. 2. Simultaneous measurement system: photoacoustic measurement of viscoelastic characteristics and fluorescent measurement with time-resolved autofluorescence spectroscopy. From a practical perspective, a commercially available 3rd (355 nm) harmonic Q-switched Nd:YAG laser (pulse width, 5–6 nanoseconds) was used for the excitation light source in the present study. The light beam was focused with a lens and then coupled to a silica fiber of 400 μm in core diameter. Transmitted light energy was maintained at approximately 50 μJ/pulse. Thermoelastic waves induced by the light pulses were detected by a piezoelectric transducer we designed ourselves, which consisted of a P(VdF/TrFE) film of 55 μm in thickness. Output signals of the transducer were amplified with a low-noise amplifier (bandwidth, 1 kHz–100 MHz; gain, 46 dB) and acquired with a multi-channel digital oscilloscope (bandwidth, 1 GHz). The relaxation time, calculated as the time for the thermoelastic wave amplitude to decrease by a factor of $1/e$, gave the relaxation parameters ($\eta/G$) of tissue, where $\eta$ is viscosity and $G$ is elasticity. Time-resolved fluorescent spectroscopy was obtained by a photonic multi-channel analyzer with intensified CCD. For time-resolved measurement, a trigger signal was controlled by a 4-channel digital signal generator. Fluorescent features of the developed measurement system are as follows: wavelength range, 200–860 nm; wavelength resolution <3 nm; exposure time, 19 milliseconds; gate time, 10 nanoseconds. The parameters of measured fluorescence, obtained using MatLab software, were peak wavelength at fluorescence maximum, fluorescent spectral bandwidth at half-maximal amplitude (FWHM), and integrated intensity of time-resolved spectrum. The figure was cited and modified from Bioengineering: Principles, Methodologies, and Applications ISBN: 978-1-60741-762-0 Authors: M. Sato et al., Editors: A. Garcia et al., pp. 179–190, 2010 Nova Science Publishers, Inc. Chapter 7.

## Safety Test

To assess the safety of the photoacoustic measurement method, we used a cell proliferative activity test in cultivated domestic rabbit chondrocytes and examined the effects on chondrocytes of laser beam irradiation to induce photoacoustic signals. As irradiation conditions of the laser were based on the third harmonic frequency of a Q switch Nd:YAG laser with a wavelength of 355 nm, the following five groups were established and examined: (1) a group treated under clinically used radiation conditions (100 μJ/mm$^2$, 30 shots, $n = 6$); (2) a group treated under conditions in which the pulse energy was 1.5-times greater than that used clinically (150 μJ/mm$^2$, 30 shots, $n = 6$); (3) a group treated under conditions in which the number of pulse shots was 50 times higher than the

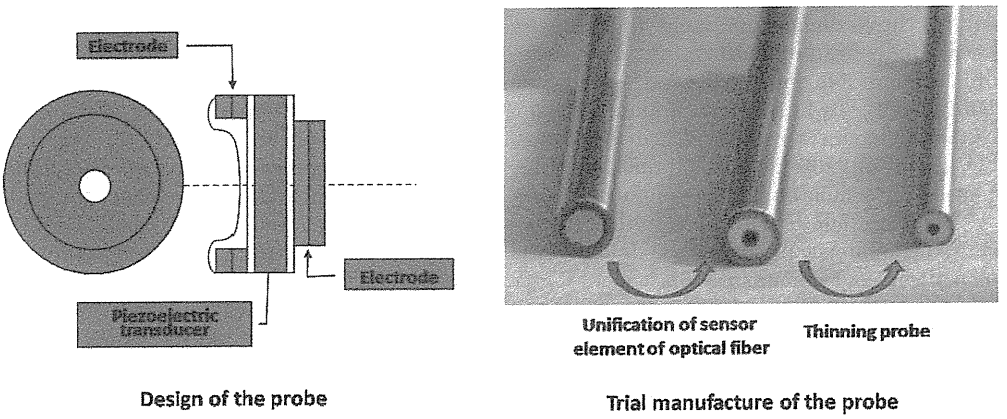


Fig. 3. Development of the probes. We developed a probe in which the optical output was introduced via a quartz glass optical fiber (core diameter 400 nm; Thorlabs Japan), and the P (VdF/TrFE) of a piezoelectric polymer film was used to detect the photoacoustic waves. In this polymer film, the laser irradiation side and the measuring side were originally opposite, so only transparent objects could be evaluated in vitro. However, with repeated trial and error, we developed an integrated optical fiber reflective probe that allowed measurements to be made in vivo, specifically during arthroscopy, by situating the probe at the center and placing the sensors peripherally around it in a circle. The figure was cited and modified from Bioengineering: Principles, Methodologies, and Applications ISBN: 978-1-60741-762-0 Authors: M. Sato et al., Editors: A. Garcia et al., pp. 179–190, 2010 Nova Science Publishers, Inc. Chapter 7.

number used clinically (150 $\mu J/mm^2$, 1,500 shots, $n = 6$); (4) a positive control group to which 70% ethanol was added to completely kill the cells ($n = 4$); and (5) a negative control with no laser irradiation ($n = 4$). Notably, the pulse energy used to treat group (2) represented the maximum output of this device. A WST-8 assay (Dojindo Laboratories, Kamimashiki, Kumamoto, Japan) was used for the cell proliferative activity test. We applied the abovementioned conditions to cultivated cells sown in a 96-well plate and cultured at 37°C under 5% $CO_2$, with all measurements made after 1 hour.

## Comparative Studies of Mechanical Properties for Tissue-Engineered Cartilage Measured by Photoacoustic Method and Intrinsic Viscoelastic Measurements

**Tissue-engineered cartilage made from chondrocytes cultured using scaffold.** Twelve knee joints were obtained from 4-week-old female Japanese White rabbits, each weighing about 1 kg. Articular cartilage was separated from the joint with a scalpel and digested for 4 hours in Dulbecco's modified Eagle's medium (DMEM) (Nissui Pharmaceutical, Tokyo, Japan) containing 0.0125% (w/v) bacterial collagenase P (Roche, Mannheim, Germany) and 0.05% actinase E (Kaken Pharmaceutical, Tokyo, Japan). The digested tissue was passed through a cell strainer (BD Biosciences, Wobum, MA) with a pore size of 40 μm. The filtrate was centrifuged at 1,500 rpm for 10 minutes to separate the cells. Cells were then seeded at high density ($1 \times 10^6$ cells per scaffold) into an ACHMS scaffold (atelocollagen honeycomb with a membrane seal; diameter, 11 mm; thickness, 2 mm) [41,43,44], which we

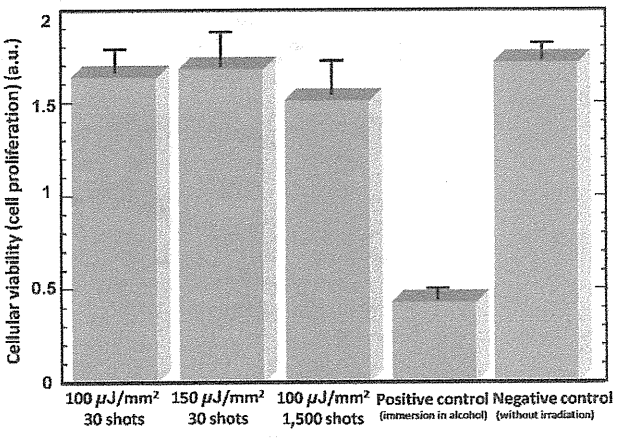


Fig. 4. Effect of laser irradiation (energy per $mm^2$) on cell viability (cell proliferation). Results of a cell proliferation assay using WST-8. Data were obtained 1 hour after incubation and inoculation. Group A: 100 $mJ/mm^2$, 30 shots (this condition is standard in our studies). Group B: 150 $mJ/mm^2$, 30 shots (this condition represents maximum fluence of this laser system). Group C: 100 $mJ/mm^2$, 1,500 shots. Group D: Positive control (immersion in alcohol). Group E: Negative control without irradiation. Error bars show standard deviation ($n = 4$–6). Results for Group E showed no significant differences from those for the other laser irradiation groups (Groups A–C). The figure was cited and modified from Lasers in Surgery and Medicine 38:249–255 (2006) Authors: M. Ishihara, M. Sato et al.

had developed for three-dimensional and high-density culture in 48-well plates (Sumitomo Bakelite, Tokyo, Japan) by centrifugation at 500 rpm for 5 minutes and then cultured in DMEM-F12 (Iwaki, Tokyo, Japan) supplemented with 10% fetal bovine serum at 37°C in an atmosphere of 5% $CO_2$ in air and 100% relative humidity. After the indicated periods of incubation, tissue-engineered cartilages using ACHMS scaffold (Fig. 5) were studied biomechanically using the photoacoustic method ($n = 6$) and intrinsic viscoelastic measurements ($n = 6$).

### Biomechanical Study

**Photoacoustic method.** The third harmonic frequency of a Q switch Nd:YAG laser (wavelength, 355 nm; pulse width, 5–6 nanoseconds; Excel Technology, Tokyo, Japan) was used at a constant repetition rate of 10 Hz. The beam was focused using a lens and then coupled to a silica fiber with a core diameter of 400 μm. Transmitted light energy was maintained at approximately 50 μJ/pulse. Stress waves induced by the light pulses were detected at the back surface of the sample by a piezoelectric transducer consisting of P(VdF/TrFE) film, 4 mm in diameter and 55 μm in thickness. Output signals of the photoacoustic transducer were amplified using a low-noise amplifier (bandwidth, 1 kHz–100 MHz; gain, 46 dB) and acquired with a multichannel digital oscilloscope (bandwidth, 1 GHz). Relaxation time $T$, which was calculated as the time required for stress wave amplitude to

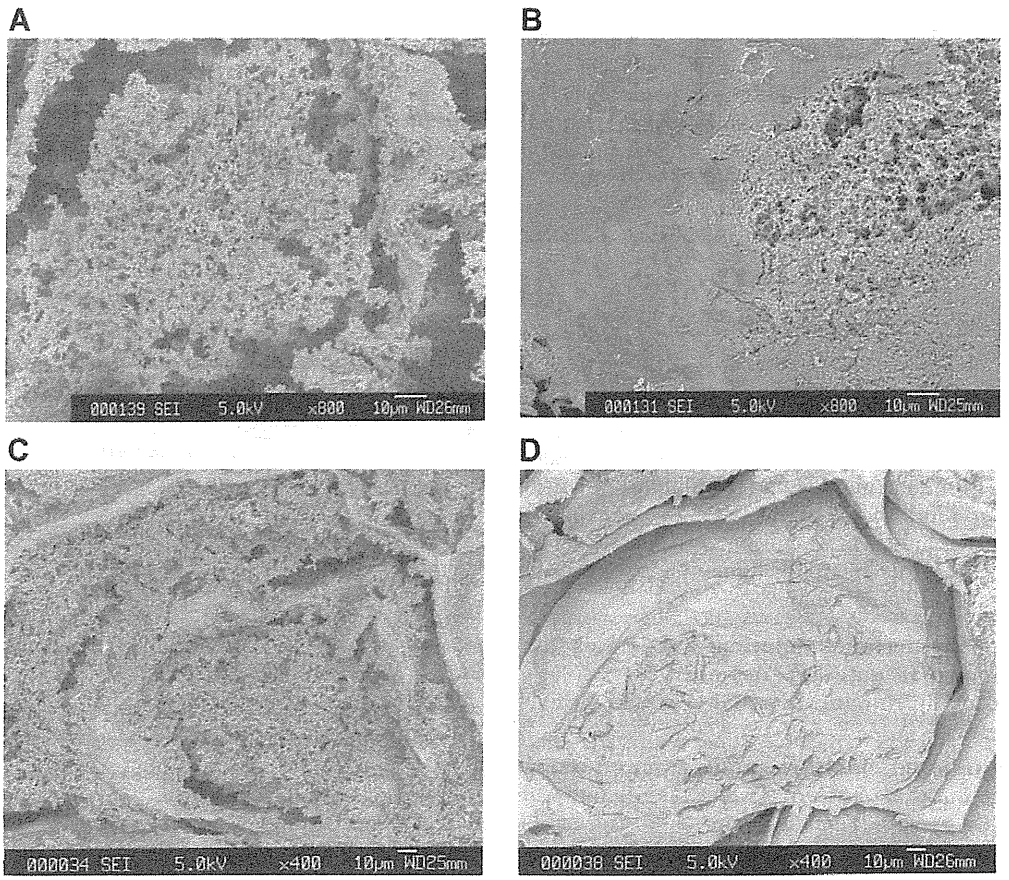


Fig. 5. Tissue-engineered cartilage using ACHMS scaffold. This figure shows a comparison of scanning electron microscopic (SEM) images of tissue-engineered cartilage cultured for 3 and 12 weeks. The lower magnification image of cartilage cultured for 3 weeks (**C**) shows a loose extracellular matrix in the honeycomb-shaped partition. In the higher-magnification image of cartilage cultured for 3 weeks (**A**), a network of collagen fibrils and interspersed proteoglycan is shown. In the images of cartilage cultured for 12 weeks (**B** and **D**), a tight extracellular matrix in the honeycomb partition is shown. Images differ considerably from those of cartilage cultured for 3 weeks, in which collagen and proteoglycan cannot be distinguished. Formation of an extracellular matrix is obvious. The figure was cited from Tissue Engineering Volume 11, Number 7/8, 2005, Mary Ann Liebert, Inc. Authors: M. Ishihara, M. Sato et al.

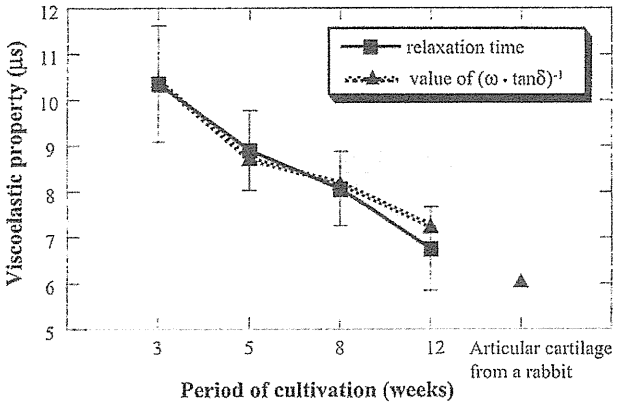


Fig. 6. Comparison of relaxation times measured by the photoacoustic method and values of $(\omega \cdot \tan \delta)^{-1}$ (intrinsic viscoelastic properties) measured with a rheometer as a function of culture time ($\omega = 0.75$ MHz). (■) Relaxation times; (▲) values of $(\omega \cdot \tan \delta)^{-1}$. The correlation coefficient is 0.98. Error bars indicate the standard deviation. To compare viscoelasticities of engineered tissue and native tissues, the value of $(\text{cotan } \delta)^{-1}$ for articular cartilage from a rabbit is plotted ($n = 6$). The figure was cited and modified from Tissue Engineering Volume 11, Number 7/8, 2005, Mary Ann Liebert, Inc. Authors: M. Ishihara, M. Sato et al.

decrease by a factor of $1/e$, was measured. Relaxation time shows a relationship with the viscous-to-elastic modulus rate (tan $\delta$) when $\omega$ is defined as the frequency of a stress wave: $T = (\omega \cdot \tan \delta)^{-1}$ [31].

**Intrinsic viscoelastic measurements.** Intrinsic viscoelastic properties of the same samples as those used for the photoacoustic measurements were examined with a rheometer, a conventional viscoelastic analyzer, and the data were compared to those obtained using the photoacoustic method. Measurements using a rheometer were made at an environmental temperature of 20°C and an initial stress of 80 Pa [31].

The recorded waveform of the photoacoustic signal of the engineered cartilages cultured for 12 weeks is shown in the monitor of a digital oscilloscope in Figure 2. The signal shows a pulse sequence that is due to multiple acoustic reflections at the acoustic boundaries. When attenuation of the stress wave intensity is affected only by reflection at the boundaries and relaxation during transmission through the viscoelastic material, the peak intensity of each wave packet is expressed as an exponential function. Using the Levenberg–Marquardt algorithm, a nonlinear least-squares method, relaxation time can be derived as the time for the stress wave intensity to decrease by a factor of $1/e$.

**Evaluation of degenerated cartilage.** To produce experimentally degenerated cartilage, we created cartilage with different degrees of degradation by extracting 22 osteochondral plugs (diameter, 12 mm) from four swine patellar cartilage and processing them with trypsin (trypsin-1 × EDTA; Invitrogen, Carlsbad, CA) to cause an outflow of proteoglycan, reflecting changes in the mechanical characteristics of the tissue in vivo. Trypsin was applied for up to 24 hours at a concentration of 1 mg/ml. We assessed degenerated cartilage using the photoacoustic measurement method. After measurements had been made, samples were fixed in 10% formalin solution for histological study. Samples (0 hours: $n = 6$, 6 hours: $n = 6$, 12 hours: $n = 6$, 24 hours: $n = 4$) were sectioned to 4-μm thick slices for microscopic observation and stained with toluidine blue.

### Evaluation of Osteochondral Defects in Rabbit Articular Cartilage Using Photoacoustic Measurement Method

We demonstrated the capability of photoacoustic measurement for viscoelastic characterization. Since tissue viscoelasticity affects the propagation and attenuation of photoacoustic waves generated in the tissue, the relaxation times of the photoacoustic waves give the viscoelastic ratio of the tissue. The relaxation times of photoacoustic waves of articular cartilage tissues engineered under various culture conditions were closely correlated with intrinsic viscoelastic ratio measured by using a conventional viscoelastic analyzer ($R > 0.98$, Fig. 6). In order to apply the photoacoustic measurement method to evaluation of the regeneration of articular cartilage as a method to validate the surgery, the method should enable not only evaluation of engineered tissue during cultivation in vitro but also evaluation after transplantation of engineered tissue in vivo. We performed regenerative medicine using the rabbit osteochondral defect model and tissue engineered cartilage using ACHMS scaffold ($n = 8$, Fig. 5).

### Evaluation of Cartilage Using Time-Resolved Autofluorescence Spectroscopy

For time-resolved autofluorescence spectroscopy, we used the third harmonic frequency of the Q switch Nd:YAG laser for the excitation light introduced via an optic fiber, in a manner similar to that used in the photoacoustic measurement method. We used a charge-coupled device (CCD) sensor with an image intensifier as the photodetector, while controlling the spectroscopic system that could be measured by a nanosecond order with a 4-channel digital pulse generator. Fluorescence peak intensity, half bandwidth, peak wavelength, fluorescence volume, and fluorescence life were calculated as the measurement parameters. The articular cartilage of Japanese white domestic rabbits ($n = 4$), the outer layer of the annulus fibrosus ($n = 4$), and commercially available type I and type II collagen (powder; Ieda Chemical, Tokyo, Japan, $n = 4$, respectively) were used as the target samples.

## RESULTS

### Determination of Optimal Wavelength

Photoacoustic signals could thus be measured at any wavelength within this range [29,31]. The shorter wavelengths within this range can magnify absorption by

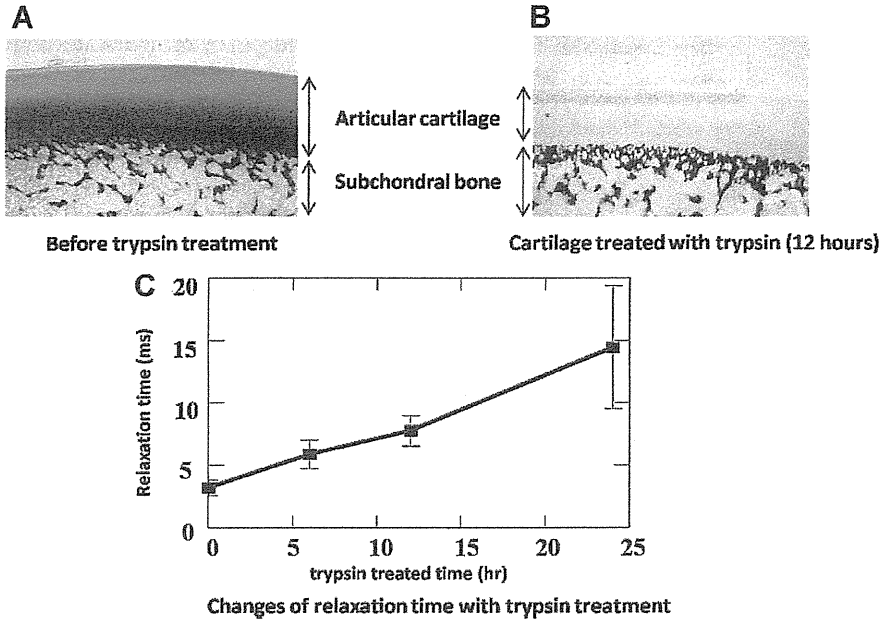


Fig. 7. Photoacoustic evaluation of characteristic viscoelastic changes with cartilage degeneration. Trypsin treatment of the tissue caused marked loss of proteoglycans in the cartilage, as shown in **A** and **B**. (a) Toluidine blue staining of a normal porcine cartilage specimen. (b) Toluidine blue staining of a cartilage specimen treated with trypsin for 12 hours. The specimen shows an extensive loss of proteoglycans in the tissue. Changes in the extracellular matrix simultaneously caused change in viscoelasticity of the cartilaginous tissue. The degree of change in viscoelasticity corresponded to the degree of change in the extracellular matrix. **C**: Relaxation times measured by the photoacoustic measurement method as a function of trypsin treatment time (hours). Error bars show standard deviation (0 hours: $n = 6$, 6 hours: $n = 6$, 12 hours: $n = 6$, 24 hours: $n = 4$). The figure was cited and modified from Lasers in Surgery and Medicine 38:249–255 (2006) Authors: M. Ishihara, M. Sato et al.

living organs, so peak values of the initiated photoacoustic waves can be increased and the initiation depth of the photoacoustic wave set at a shallower level. However, in practical terms, a small, portable, and inexpensive excitation light source is desirable, so we devised a system in which the third harmonic frequency of a Q switch Nd:YAG laser (wavelength, 355 nm; pulse width, 5–6 nanoseconds; Excel Technology) was used [39,40]. We developed a probe in which the optical output was introduced via a quartz glass optical fiber (core diameter, 400 nm; Thorlabs Japan, Tokyo, Japan), and the poly(polyvinylidene fluoride) copolymer (P(VdF/TrFE)) of a piezoelectric polymer film (Nishiki Trading Company, Tokyo, Japan) was used to detect the photoacoustic waves [40]. In this polymer film, the laser irradiation side and measuring side were originally opposite, so only transparent objects were able to be evaluated in vitro. However, with repeated trial and error, we developed an integrated optical fiber reflective probe that allowed measurements to be taken in vivo, specifically during arthroscopy, by situating the probe at the center and placing the sensors peripherally around the probe in a circle (Fig. 3).

### Effect of Laser Irradiations

We confirmed a lack of significant differences between any laser-irradiated group and the non-irradiated group, and found that laser irradiation in this study had no effect on cell proliferative activity (Fig. 4) [40].

### Mechanical Properties of Tissue-Engineered Cartilage Measured by Photoacoustic Method and Intrinsic Viscoelastic Measurements

In Figure 6, relaxation times are compared to intrinsic viscoelastic parameters (tan $\delta$) measured with a rheometer. The intrinsic relaxation parameter of native cartilage measured with the rheometer is also plotted in Figure 6. Tissue-engineered cartilage cultured for a longer period showed smaller relaxation times. The relaxation times obtained by photoacoustic measurement agreed well with the measured intrinsic relaxation parameters, with a correlation coefficient of 0.98. Compared to native cartilage,

cartilage cultured for the longest period (12 weeks) showed an 85% smaller viscoelastic parameter [31].

### Photoacoustic Evaluation of Characteristics of Degenerated Cartilage

Figure 7 shows the positive correlation between damping time and trypsinization time [40]. Specifically, damping time increased with increasing trypsinization time. In other words, viscosity increased and elasticity decreased. Histologically, the stainability of tissue with toluidine blue also decreased with trypsinization and the loss of proteoglycans, suggesting that the course of tissue changes involved in cartilage degeneration can be monitored using the photoacoustic measurement method.

### Monitoring the Post-Operative Regenerative Process of Articular Cartilage Using Photoacoustic Measurement Method

We confirmed that the usefulness of the photoacoustic method for repeated measurement of viscoelastic properties of regenerative articular cartilage after allografted tissue-engineered cartilage. The photoacoustic measurements enabled the determinations of viscoelasticities of regenerative cartilage during the total time course after surgery (Fig. 8).

### Compositional Information of Cartilage Using Time-Resolved Autofluorescence Spectroscopy

The articular cartilage exhibited a spectrum close to that of type II collagen, and peak wavelengths and half bandwidths were also similar [33,38]. Conversely, the outer layer of the annulus fibrosus exhibited a spectrum close to that of type I collagen, and peak wavelengths and half bandwidths were also similar (Fig. 10) [42,43]. This indicates that the collagen composition of tissue can be measured, as collagen is an autofluorescent substance used in vivo in a non-contact manner. This is significant, as the content ratio of type I to type II collagen is particularly important in diagnosing the degree of cartilage degradation.

## DISCUSSION

Based on the above results, we applied the photoacoustic measurement method to evaluate the articular cartilage under the arthroscopy. We received the approval of the Institutional Review Board of Tokai University Hospital concerning the photoacoustic measurement method, and applied the method to some kinds of arthroscopic surgeries. The surgeon can easily have a true figure of photoacoustic waveform using the real-time monitoring. The measuring photoacoustic waveform in the monitor can be changed to make larger or smaller by switching (Fig. 9). The measurable thickness was limited from approximately 1.5 to 6 mm in the present experimental condition. In this range of the cartilage thickness, the effect of the thickness on the accuracy of the measurement was ignorable.

Many elderly people who suffer from lifestyle-related diseases are also affected by osteoarthritis and are often unable to perform exercises that would normally be within their physical capacity, due to joint pain and limited range of motion. This is particularly serious in patients with diabetes, hyperlipidemia, or obesity, and the disease may be exacerbated because osteoarthritis reduces the ability to exercise, even when exercise therapy is available. In osteoarthritis, evaluating the prognosis of conservative therapy or the treatment effects after surgery often depend on the symptoms of the

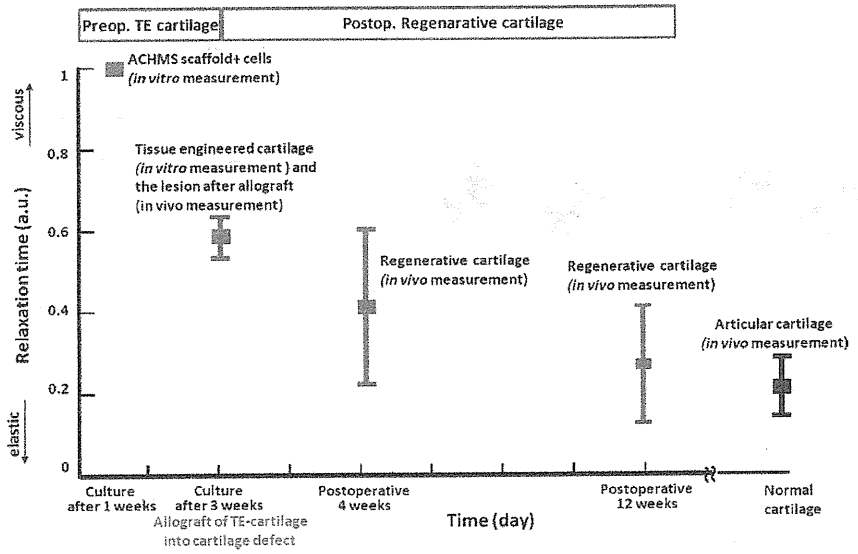


Fig. 8. The results of photoacoustic measurement of pre- and post-operative cartilage. A total time course of pseudo-regenerative medicine using rabbit model was able to be monitored by photoacoustic method.

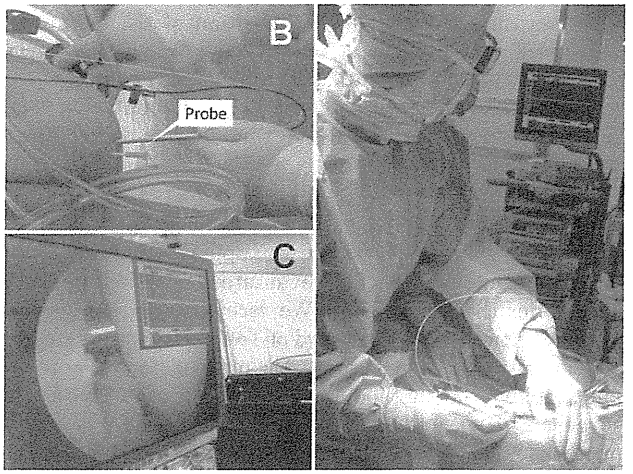


Fig. 9. Clinical application of photoacoustic measurement. A: The measuring photoacoustic waveform can be checked by the monitor of arthroscopy. B: The integrated optical fiber of reflective probe was 4mm in diameter (Fig. 3). C: The measuring photoacoustic waveform in the monitor can be changed to make larger or smaller by switching.

patient, so the pathological condition is not accurately understood. Surgical treatments such as artificial joint replacement are currently performed on patients in the terminal phase, whereas patients in the initial to middle phases are treated conservatively, often without any clear aims.

The present studies have demonstrated that the mechanical characteristics and properties of articular cartilage can be evaluated simultaneously during arthroscopy using a non-invasive intense pulsed laser (Table 1). We are now developing a device for this application by trial and error. If such a device is developed, accurate measurement of the mechanical characteristics involved with the original function of the articular cartilage and the associated tissue properties will be possible during arthroscopy, and anyone could perform such quantitative functional evaluations. This will enable an accurate understanding of the pathological features of osteoarthritis and careful planning and implementation of treatments. This technology could also allow quantitative measurement and evaluation of mechanical characteristics and tissue properties simultaneously, to assess treatment effects such as those of a variety of drugs, in

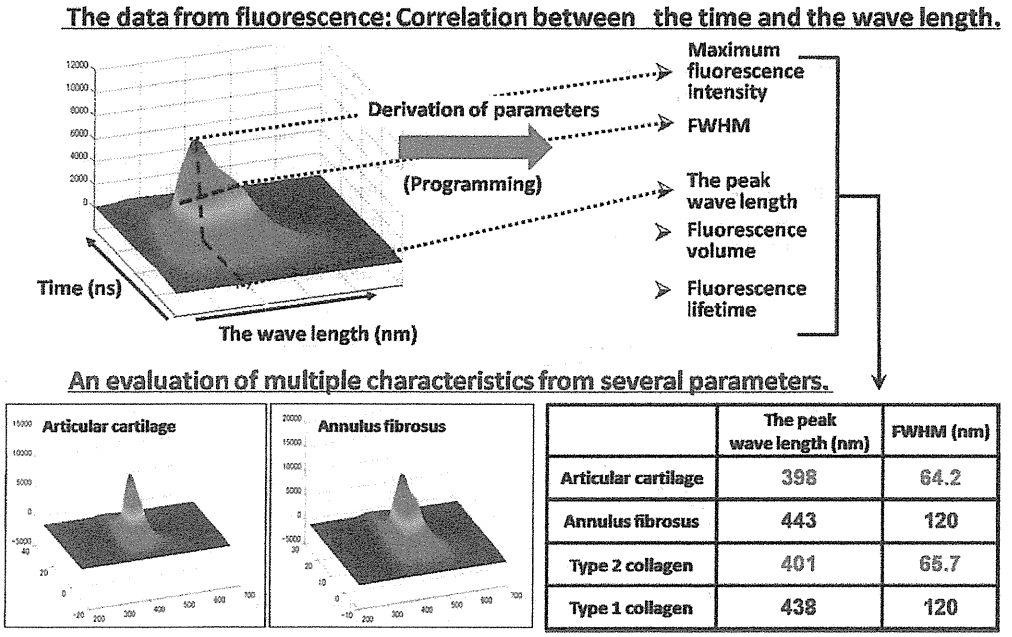


| | The peak wave length (nm) | FWHM (nm) |
|---|---|---|
| Articular cartilage | 398 | 64.2 |
| Annulus fibrosus | 443 | 120 |
| Type 2 collagen | 401 | 65.7 |
| Type 1 collagen | 438 | 120 |

Fig. 10. Analyses with time-resolved autofluorescence spectroscopy. Fluorescence peak intensity, full width at half maximum (FWHM), peak wavelength, fluorescence volume, and fluorescence life were calculated as the measurement parameters. The articular cartilage of Japanese white domestic rabbits, the outer layer of the annulus fibrosus, and commercially available type I and type II collagen were used as target samples. Articular cartilage exhibited a spectrum close to that of type II collagen, and peak wavelengths and half bandwidths were also similar. Conversely, the outer layer of the annulus fibrosus exhibited a spectrum close to that of type I collagen, and peak wavelengths and half bandwidths were also similar. This indicates that the collagen composition of tissue can be measured, as collagen is an autofluorescent substance used in vivo in a non-contact manner. The figure was cited and modified from Bioengineering: Principles, Methodologies, and Applications ISBN: 978-1-60741-762-0 Authors: M. Sato et al., Editors: A. Garcia et al., pp. 179–190, 2010 Nova Science Publishers, Inc. Chapter 7.

addition to the conventional evaluation of clinical symptoms such as pain or inflammation around the joints. We believe that this methodology will be useful in the objective evaluation of articular cartilage in investigations such as clinical trials of new drugs. This diagnostic system is a methodology used during arthroscopy, and so cannot be a completely non-invasive evaluation [41]. However, if quantitative data are collected during arthroscopy treatments, the effects of a variety of conservative therapies will be able to be predicted, based on the severity of cartilage degeneration. Planning and performance of treatments on an individual basis will thus be possible. Accordingly, we are certain that the development of this technology and practical diagnostic devices will improve activities of daily living and quality of life for patients, and thus contribute to a healthy life expectancy.

## CONCLUSION

1. A photoacoustic measurement method using a non-invasive nanosecond-pulsed laser allows evaluation of the mechanical characteristics of cartilage, and time-resolved autofluorescence spectroscopy allows the evaluation of tissue properties for analysis.
2. This measurement system, based on interactions between optics and living organs, is an evaluation methodology suitable for making diagnoses during arthroscopy.

## ACKNOWLEDGMENTS

This work was supported by the Takeda Science Foundation, the General Insurance Association of Japan, Mitsui Sumitomo Insurance Welfare Foundation, a High-Tech Research Centre Project for Private Universities, a grant-in-aid for Scientific Research from the Ministry of Education, Culture, Sports, Science, and Technology of Japan, the New Energy and Industrial Technology Development Organization, and the Japan Foundation for Aging and Health.

## REFERENCES

1. Yoshimura N, Oka T, Muraki S, Mabuchi A, Enyo Y, Yoshida M, Kawaguchi H, Nakamura K. Epidemiology of osteoarthritis in Japan. J Jpn Orthop Assoc 2007;81:17–21.
2. Modest VE, Murphy MC, Mann RW. Optical verification of a technique for in situ ultrasonic measurement of articular cartilage thickness. J Biomech 1989;22:171–176.
3. Rushfeldt PD, Mann RW, Harris WH. Improved techniques for measuring in vitro the geometry and pressure distribution in the human acetabulum-I. Ultrasonic measurement of acetabular surfaces, sphericity and cartilage thickness. J Biomech 1981;14:253–260.
4. Kim HK, Babyn PS, Harasiewicz KA, Gahunia HK, Pritzker KP, Foster FS. Imaging of immature articular cartilage using ultrasound backscatter microscopy at 50 MHz. J Orthop Res 1995;13:963–970.
5. Adler RS, Dedrick DK, Laing TJ, Chiang EH, Meyer CR, Bland PH, Rubin JM. Quantitative assessment of cartilage surface roughness in osteoarthritis using high frequency ultrasound. Ultrasound Med Biol 1992;18:51–58.
6. Laasanen MS, Töyräs J, Hirvonen J, Saarakkala S, Korhonen RK, Nieminen MT, Kiviranta I, Jurvelin JS. Novel mechano-acoustic technique and instrument for diagnosis of cartilage degeneration. Physiol Meas 2002;23:491–503.
7. Nieminen HJ, Töyräs J, Rieppo J, Nieminen MT, Hirvonen J, Korhonen R, Jurvelin JS. Real-time ultrasound analysis of articular cartilage degradation in vitro. Ultrasound Med Biol 2002;28:519–525.
8. Toyras J. Quantitative evaluation of spontaneously and surgically repaired rabbit articular cartilage using intra-articular ultrasound method in situ. Ultrasound Med Biol 2010;36:833–839.
9. Bader DL, Kempson GE. The short-term compressive properties of adult human articular cartilage. Biomed Mater Eng 1994;4:245–256.
10. Korhonen RK, Laasanen MS, Toyras J, Lappalainen R, Helminen HJ, Jurvelin JS. Fibril reinforced poroelastic model predicts specifically mechanical behavior of normal, proteoglycan depleted and collagen degraded articular cartilage. J Biomech 2003;36:1373–1379.
11. Froimson MI, Ratcliffe A, Gardner TR, Mow VC. Differences in patellofemoral joint cartilage material properties and their significance to the etiology of cartilage surface fibrillation. Osteoarthritis Cartilage 1997;5:377–386.
12. Maroudas A, Evans H, Almeida L. Cartilage of the hip joint. Topographical variation of glycosaminoglycan content in normal and fibrillated tissue. Ann Rheum Dis 1973;32:1–9.
13. Hattori K, Mori K, Habata T, Takakura Y, Ikeuchi K. Measurement of the mechanical condition of articular cartilage with an ultrasonic probe: Quantitative evaluation using wavelet transformation. Clin Biomech (Bristol, Avon) 2003; 18:553–557.
14. Hattori K, Ikeuchi K, Morita Y, Takakura Y. Quantitative ultrasonic assessment for detecting microscopic cartilage damage in osteoarthritis. Arthritis Res Ther 2005;7:R38–R46.
15. Appleyard RC, Swain MV, Khanna S, Murrell GA. The accuracy and reliability of a novel handheld dynamic indentation probe for analysing articular cartilage. Phys Med Biol 2001;46:541–550.
16. Bae WC, Temple MM, Amiel D, Coutts RD, Niederauer GG, Sah RL. Indentation testing of human cartilage: Sensitivity to articular surface degeneration. Arthritis Rheum 2003; 48:3382–3394.
17. Lyyra T, Jurvelin J, Pitkänen P, Väätäinen U, Kiviranta I. Indentation instrument for the measurement of cartilage stiffness under arthroscopic control. Med Eng Phys 2003;17: 395–399.
18. Viren T, Saarakkala S, Kaleva E, Nieminen HJ, Jurvelin JS, Toyras J. Minimally invasive ultrasound method for intra-articular diagnostics of cartilage degeneration. Ultrasound Med Biol 2009;35:1546–1554.
19. Huang YP, Zheng YP. A potential arthroscopic tool for quantitative assessment of articular cartilage. Open Biomed Eng J 2009;26:13–20.
20. Viren T, Saarakkala S, Jurvelin JS, Pulkkinen HJ, Tiitu V, Valonen P, Kiviranata I, Lammi MJ, Xia Y, Moody JB, Burton-Wurster N, Lust G. Quantitative in situ correlation between microscopic MRI and polarized light microscopy studies of articular cartilage. Osteoarthritis Cartilage 2001; 9:393–406.
21. Li X, Martin S, Pitris C, Ghanta R, Stamper DL, Harman M, Fujimoto JG, Brezinski ME. High-resolution optical coherence tomographic imaging of osteoarthritic cartilage during open knee surgery. Arthritis Res Ther 2005;7:R318-23.
22. Chu CR, Izzo NJ, Irrgang JJ, Ferretti M, Studer RK. Clinical diagnosis of potentially treatable early articular cartilage degeneration using optical coherence tomography. J Biomed Opt 2007;12:051703.
23. Burstein D, Gray M. New MRI techniques for imaging cartilage. J Bone Joint Surg Am 2003;85-A(Suppl 2): 70–77.
24. Nieminen MT, Toyras J, Rieppo J, Hakumäki JM, Silvennoinen J, Helminen HJ, Jurvelin JS. Quantitative MR microscopy of enzymatically degraded articular cartilage. Magn Reson Med 2000;43:676–681.

25. Nieminen MT, Rieppo J, Töyräs J, Hakumäki JM, Silvennoinen J, Hyttinen MM, Helminen HJ, Jurvelin JS. T2 relaxation reveals spatial collagen architecture in articular cartilage: A comparative quantitative MRI and polarized light microscopic study. Magn Reson Med 2001;46:487–493.
26. Xia Y, Moody JB, Burton-Wurster N, Lust G. Quantitative in situ correlation between microscopic MRI and polarized light microscopy studies of articular cartilage. Osteoarthritis Cartilage 2001;9:393–406.
27. Bashir A, Gray ML, Hartke J, Burstein D. Nondestructive imaging of human cartilage glycosaminoglycan concentration by MRI. Magn Reson Med 1999;41:857–865.
28. Nieminen MT, Rieppo J, Silvennoinen J, Töyräs J, Hakumäki JM, Hyttinen MM, Helminen HJ, Jurvelin JS. Spatial assessment of articular cartilage proteoglycans with Gd-DTPA-enhanced T(1) imaging. Magn Reson Med 2002;48: 640–648.
29. Ishihara M, Sato M, Sato S, Kikuchi T, Fujikawa K, Kikuchi M. Viscoelastic characterization of biological tissue by photoacoustic measurement. Jpn J Appl Phys 2003;42:556–558.
30. Ishihara M, Sato M, Sato S, Kikuchi T, Mitani G, Kaneshiro N, Mochida J, Kikuchi M. Usefulness of the photoacoustic measurement method for monitoring the regenerative process of full-thickness defects in articular cartilage using tissue-engineering technology. Progress in biomedical optics and imaging. Proc SPIE 2005;5695:288–291.
31. Ishihara M, Sato M, Sato S, Kikuchi T, Mochida J, Kikuchi M. Usefulness of photoacoustic measurements for evaluation of biomechanical properties of tissue-engineered cartilage. Tissue Eng 2005;11:1234–1243.
32. Ishihara M, Sato M, Ishihara M, Mochida J, Kikuchi M. Multifunctional Evaluation of Tissue Engineered Cartilage Using Nano-Pulsed Light for Validation of Regenerative Medicine. In: Kim SI, Suh TS (editors). IFMBE Proceedings, World Congress on Medical Physics and Biomedical Engineering 14; August 27–September 1; COEX Seoul, Korea. Springer: Berlin, Heidelberg, 2006: 3187–3189.
33. Ishihara M, Sato M, Kaneshiro N, Mitani G, Sato S, Ishihara M, Mochida J, Kikuchi M. Development of a noninvasive multifunctional measurement method using nanosecond pulsed laser for evaluation of regenerative medicine for articular cartilage. Proc SPIE 2006;6084:60840V.1–60840V.4.
34. Ishihara M, Sato M, Kaneshiro N, Mitani G, Nagai T, Kutsuna T, Mochida J, Kikuchi M. Usefulness and limitation of measurement methods for evaluation of tissue-engineered cartilage function and characterization using nanosecond pulsed laser. Proc SPIE 2007;6439:643909.1–643909.4.
35. Ishihara M, Sato M, Mitani G, Mochida J, Kikuchi M. Monitoring of extracellular matrix formation using nanosecond pulsed laser. J Inst Elect Engnr Jpn 2007;127-C:2166–2170.
36. Ishihara M, Sato M, Mochida J, Kikuchi M. Measurement and image engineering for fundamental technology of regenerative medicine. In: Akaike T, ed. Regeneration Medicine 4, Bioengineering for Regeneration Medicine. Tokyo: Corona Publishing 2007: 147–167.
37. Ishihara M, Sato M, Mochida J, Kikuchi M. Noninvasive measurement for the evaluation and validation of regeneration medicine. J Biosci Biotechnol 2007;85:438–441.
38. Ishihara M, Sato M, Kutsuna T, Ishihara M, Mochida J, Kikuchi M. Modification of measurement methods for evaluation of tissue engineered cartilage function and biochemical properties using nanosecond pulsed laser. Proc SPIE 2008; 6558:685805.1–685805.5.
39. Ishihara M, Sato M, Kaneshiro N, Mitani G, Sato S, Mochida J. Development of a photoacoustic measurement method for the evaluation of regenerative medicine and tissue engineering for articular cartilage. J Jpn Soc Laser Surg Med 2005; 26:53–59.
40. Ishihara M, Sato M, Kaneshiro N, Mitani G, Sato S, Mochida J. Development of a diagnostic system for osteoarthritis using a photoacoustic measurement method. Lasers Surg Med 2006;38:249–255.
41. Sato M, Ishihara M, Furukawa K, Kaneshiro N, Nagai T, Mitani G, Kutsuna T, Ohta N, Kokubo M, Kikuchi T, Sakai H, Ushida T, Kikuchi M, Mochida J. Recent technological advancements related to articular cartilage regeneration. Med Biol Eng Comput 2008;46:735–743.
42. Han C, Barnett B. Measurement of the rheological properties. In: Gabelnick HL, Litt M (editors). Rheology of Biological Systems. Illinois: Charles C. Thomas; pp. 95–217. In: Kim SI, Suh TS (editors). IFMBE Proceedings, World Congress on Medical Physics and Biomedical Engineering 14; August 27–September 1; COEX Seoul, Korea. Springer: Berlin, Heidelberg, 1973, 3187–3189.
43. Masuoka K, Asazuma T, Ishihara M, Sato M, Hattori H, Ishihara M, Yoshihara Y, Matsui T, Takase B, Kikuchi M, Nemoto K. Tissue engineering of articular cartilage using an allograft of cultured chondrocytes in a membrane-sealed atelocollagen honeycomb-shaped scaffold (ACHMS-scaffold). J Biomed Mater Res 2005;75B:177–184.
44. Masuoka K, Asazuma T, Hattori H, Yoshihara Y, Sato M, Matsumura K, Matsui T, Takase B, Nemoto K, Ishihara M. Tissue engineering of articular cartilage with autologous cultured adipose tissue-derived stromal cells using atelocollagen honeycomb-shaped scaffold with a membrane sealing in rabbits. J Biomed Mater Res B Appl Biomater 2006; 79:25–34.

# 関節軟骨の修復・再生における組織工学的軟骨の役割

関節軟骨の再生医療は，無血管組織であること，軟骨細胞の培養が比較的容易であったことなどから再生医療の第一世代というようないわれ方をされた時期もあった．そして軟骨の再生医療は1990年前半から海外で実施・報告され，米国をはじめとする諸外国ではすでに2万例に近い手術症例の蓄積がある．しかしながらその対象疾患は小さな軟骨の外傷性病変であり，再生医療が真に必要とされる変形性関節症の治療には，20年近く経過した現在でも，いまだに到達する気配すら感じられない．それは真の関節軟骨の再生が，想像以上にむずかしいことが明らかになってきたためで，今まさに軟骨再生医療を実現するためのブレイクスルーが待望されている．

われわれは組織工学的に構築した種々の軟骨組織を用いて，関節軟骨の修復・再生に関する基礎的研究を行い，その治療効果を動物実験で確認してきた．たとえば「スキャフォールドと培養軟骨細胞とで作製した組織工学的軟骨に関する研究」[1,2]，「スキャフォールドを用いず旋回培養法により作製した組織工学的軟骨に関する研究」[3~5]，ならびに「軟骨細胞シートによる軟骨修復・再生に関する研究」[6~11]などである．これら一連の研究により，軟骨下骨に達するような骨軟骨損傷（軟骨全層欠損）の場合は，関節軟骨の浅層部分のみを組織工学的軟骨でおおうことができれば，修復機転で動員される骨髄由来細胞と組織工学的軟骨との相互作用により，良好な軟骨修復再生がもたらされることを確認した．

軟骨細胞シートは，温度応答性培養皿を用いて作製する．この培養皿は，独自のナノ表面設計により温度応答性ポリマーを器材表面に固定化することで，器材表面は32℃を境に可逆的に疎水性（細胞培養時）と親水性（細胞シート回収時）に変化できる．この特性により，トリプシンなど細胞に損傷を与える酵素を一切用いることなく，温度を20～25℃にして10～30分程度まつだけで，無傷な細胞と細胞外マトリックスがシート状に回収可能となる．温度応答性培養皿で作製した積層化軟骨細胞シートは，通常の培養皿で得られる培養細胞とはやや異なる特性を有し，軟骨修復に適している．3層に積層化した軟骨細胞シートによる関節軟骨修復再生効果をわれわれははじめて報告し[6]，細胞シートの特性を明らかにしてきた[7,8]．作製した軟骨細胞シートそのものは力学的には脆弱ではあるが，優れた接着性を有し，損傷した軟骨からのプロテオグリカンの流出を阻止する．関節液中のカタボリックファクターから軟骨を保護し，サイトカインの持続的な供給源であるとともに，骨髄由来幹細胞の軟骨分化を促進するイニシエータとしても機能しており，単なる軟骨再生というよりは，むしろ自己修復能力を向上させる効果により，軟骨は修復・再生されている．さらに従来再生医療が適用とされてきた軟骨全層欠損ばかりでなく，修復困難と考えられてきた軟骨部分損傷（軟骨下骨に達しない軟骨内損傷）に対しても，細胞シートの治療効果を動物実験で確認した．これにより，変形性関節症において常に混在しながら存在する軟骨全層欠損と軟骨部分損傷の両タイプの軟骨損傷に対して，細胞シート工学という日本発のオリジナルな技術により治療できる可能性がある．変形性関節症の治療にまで踏み込んだ再生医療の実現を，われわれは目指している．

文　献


1) Masuoka K, Asazuma T, Ishihara M et al：Tissue engineering of articular cartilage using an allograft of cultured chondrocytes in a membrane-sealed atelocollagen honeycomb-shaped scaffold (ACHMS scaffold). J Biomed Mater Res Part B Appl Biomater **75**：177-184, 2005
2) Sato M, Ishihara M, Ishihara M et al：Effects of growth factors on heparin-carrying polystyrene-coated atelocollagen scaffold for articular cartilage tissue engineering. J Biomed Mater Res Part B Appl Biomater **83**：181-188, 2007
3) Nagai T, Furukawa KS, Sato M et al：Characteristics of a scaffold-free articular chondrocyte plate grown in rotational culture. Tissue Eng Part A **14**：1183-1193, 2008
4) Nagai T, Sato M, Furukawa KS et al：Optimization of allograft implantation using scaffold-free chondrocyte plates. Tissue Eng Part A **14**：1225-1235, 2008
5) Kutsuna T, Sato M, Ishihara M et al：Noninvasive evaluation of tissue-engineered cartilage with time-resolved laser-induced fluorescence spectroscopy. Tissue Eng Part C Methods **16**：365-373, 2010
6) Kaneshiro N, Sato M, Ishihara M et al：Bioengineered chondrocyte sheets may be potentially useful for the treatment of partial thickness defects of articular cartilage. Biochem Biophys Res Commun **349**：723-731, 2006
7) Kaneshiro N, Sato M, Ishihara M et al：Cultured articular chondrocytes sheets for partial thickness cartilage defects utilizing temperature-responsive culture dishes. Eur Cell Mater **13**：87-92, 2007
8) Mitani G, Sato M, Lee JI et al：The properties of bioengineered chondrocyte sheets for cartilage regeneration. BMC Biotechnol **9**：17, 2009
9) Sato M, Ishihara M, Furukawa K et al：Recent technological advancements related to articular cartilage regeneration. Med Biol Eng Comput **46**：735-743, 2008
10) Sato M：Cell sheet technologies for cartilage repair. Regenerative Medicine and Biomaterials for the Repair of Connective Tissues, ed by Archer C, Ralphs J, Woodhead Publishing, Cambridge, CRC Press, Florida, p251-265, 2010
11) 国際出願番号：PCT/JP2006/303759，出願日：2006年2月28日，出願人：(株) セルシード，東海大学，発明者：佐藤正人，坂井秀昭


（東海大学整形外科・佐藤正人）

Nagai et al. Arthritis Research & Therapy 2010, 12:R178
http://arthritis-research.com/content/12/5/R178

arthritis research&therapy

RESEARCH ARTICLE Open Access

# Intravenous administration of anti-vascular endothelial growth factor humanized monoclonal antibody bevacizumab improves articular cartilage repair

Toshihiro Nagai, Masato Sato*, Toshiharu Kutsuna, Mami Kokubo, Goro Ebihara, Naoshi Ohta, Joji Mochida

**Abstract**

**Introduction:** In this study, we investigate the efficacy of repairing an osteochondral defect in rabbit knee joints by administering bevacizumab, a humanized monoclonal anti-vascular endothelial growth factor (VEGF) antibody.

**Methods:** An osteochondral defect was created on the patellar groove of 20 Japanese white rabbits that were classified into two recipient groups: group B, administration of bevacizumab (100-mg intravenous injection on the day of surgery and 2 weeks later), and a control group (defect only). Rabbits were killed 1 and 3 months postoperatively. Sections were stained with safranin O. Repair sites were evaluated using the modified O'Driscoll International Cartilage Repair Society grading system. The expression of chondromodulin (ChM)-I and VEGF was evaluated using immunohistochemical analyses.

**Results:** At 1 month postoperatively, the repair site in group B was filled with cartilaginous tissue. At 3 months, the repair site retained this cartilage phenotype. At 1 month in the controls, the defects were mainly filled with fibrous tissue. At 3 months, the defect was replaced by fibrous tissue and bone. Over the 3-month period, histological scores were significantly higher in group B than in the controls. At 1 month, group B showed intense positive results for ChM-I in the bottom of the repair tissue. VEGF was also identified in the same area. In the controls, no ChM-I was observed in the repair tissue. Conversely, the remodeling hypertrophic chondrocyte layer stained intensely for VEGF.

**Conclusions:** Intravenous administration of bevacizumab contributes to better repair of articular cartilage in an osteochondral defect model. We suggest the possibility of facilitating articular cartilage repair with anti-VEGF antibody rather than using cultured cells or artificial scaffolds.

## Introduction

Mature articular cartilage shows limited capacity for regeneration after degeneration or injury [1]. For this reason, various treatments have been developed in anticipation of restoration by regenerative medicine. At present, techniques using penetration of subchondral bone [2-5], microfracture [6-9], mosaicplasty [10-12], cell transplantation [13-16], and implantation of tissue-engineered cartilage with various scaffold materials [17-22] or without scaffold [23-27] have been developed to overcome this obstacle. Penetration of subchondral bone such as drilling and microfracture to be filled with reparative cells from bone marrow is a method that has been developed to stimulate spontaneous healing [18]. This procedure attempts to achieve repair via the mechanism of endochondral ossification. However, the defect to be filled with reparative cells shows a large amount of vascular invasion, and the tissue tends to be replaced by bone and a surface of fibrocartilaginous repair tissue [28].

Successful regeneration of any tissue requires the presence of reparative cells with the potential to differentiate into the phenotypes required to restore the damaged

* Correspondence: sato-m@is.icc.u-tokai.ac.jp
Department of Orthopaedic Surgery, Surgical Science, Tokai University School of Medicine, 143 Shimokasuya, Isehara, Kanagawa 259-1193, Japan

site, but a microenvironment that supports the proliferation and differentiation of those cells is also needed [28,29]. In anticipation of favorable articular cartilage repair in the osteochondral defect model, reparative cells must be provided with an environment to acquire the properties of natural articular cartilage. We recently constructed a 3-D, scaffold-free, tissue-engineered cartilage [24] and transplanted this cartilage in only the superficial layer region of the osteochondral defects as an initiator of cartilage differentiation in reparative cells [23] and achieved good restoration effects in the long term [29]. We confirmed that in the early stage of transplantation, a good restoration effect of articular cartilage is seen with reparative cells derived from marrow that acquire antiangiogenic properties [23]. We therefore hypothesized that good cartilage repair may be achieved by inhibiting the bioactivity of vascular endothelial growth factor (VEGF) in the osteochondral defect. A recent investigation examined the effect of treatment with anti-VEGF humanized monoclonal antibody (bevacizumab), which was developed as a treatment for malignant tumors [30]. Bevacizumab binds to VEGF secreted by angiogenic tumors and thereby inhibits VEGF binding to the VEGF receptor in vascular endothelial cells, reportedly restraining cancer growth by inhibiting angiogenesis [31,32].

The objective of this study is to investigate the efficacy of repair in an osteochondral defect model of the rabbit knee joint following administration of bevacizumab, a humanized monoclonal anti-VEGF antibody, without using cultured cells or artificial scaffolds.

## Materials and methods

Animal experiments were approved by the ethics review board of Tokai University and were performed in accordance with the guidelines on animal use of Tokai University.

### Repair of the osteochondral defect

Twenty Japanese white rabbits (female, 16-18 weeks old, weighing approximately 3 kg) were used in this study. The rabbits were anesthetized by exposure to sevoflurane and $O_2$ gas. After receiving a medial parapatellar incision to both legs, each patella was dislocated laterally and an osteochondral defect (diameter, 5 mm; depth, 3 mm) was created on the patellar groove of the femur in both legs using a drill and a biopsy punch (Kai Industries, Seki, Japan). The bottom of the subchondral bone was shaved to a plane using the biopsy punch until bleeding was seen from the marrow. Rabbits were classified into two recipient groups: Group B, with administration of bevacizumab (10 rabbits; 100-mg intravenous injection administered on the day of surgery and 2 weeks later); and controls (10 rabbits; defect only). After recovery from surgery, all animals were allowed to walk freely in their cages without any splints.

### Histological evaluation of cartilage repair

Rabbits were killed 1 and 3 months postoperatively by an overdose of intravenous anesthetic. The distal part of the femur was excised and fixed with 4% paraformaldehyde for 7 days. Each specimen was decalcified in a solution of 10% ethylenediaminetetraacetic acid (EDTA) in distilled water (pH 7.4) for 2-3 weeks, then embedded in paraffin wax and sectioned perpendicularly (4.5-m sections) through the center of the defect. Each section was stained with safranin O for glycosaminoglycans.

Immunohistochemistry was performed as described previously [23,33]. Briefly, sections were deparaffinized according to standard procedures. Sections were treated with 0.005% proteinase (type XXIV; Sigma-Aldrich Co., St. Louis, MO, USA) for 30 min at 37°C for antigen retrieval. For chondromodulin-I (ChM-I), primary goat polyclonal antibody (Santa Cruz Biotechnology, Santa Cruz, CA, USA) diluted 1:200 in phosphate-buffered saline (PBS) and 1% bovine serum albumin (BSA) was placed on the section overnight at 4°C. For VEGF, a primary mouse monoclonal antibody (Upstate, Lake Placid, NY, USA) diluted 1:50 in PBS and 1% BSA was placed on the section overnight at 4°C. Slides were washed with PBS after incubation for 1 h at room temperature with biotin-conjugated goat antimouse secondary antibody for VEGF and with biotin-conjugated donkey antigoat secondary antibody for ChM-I. Next, slides were treated with horseradish peroxidase-labeled streptavidin for 1 h and then soaked in 0.05% solution of diaminobenzidine in Tris HCl buffer (pH 7.6) containing 0.005% hydrogen peroxide. Finally, slides were counterstained with Mayer's hematoxylin. Safranin O-stained sections were scored by two individuals under blinded conditions, according to a modified O'Driscoll [34] International Cartilage Repair Society (ICRS) grading scale [26] (Table 1).

### Statistical analysis

Results are presented as the means ± standard deviation (SD). Histological score was analyzed by the Mann-Whitney *U* test. Values of $P < 0.05$ were considered statistically significant for any differences.

## Results

### Histological evaluation of repair tissue

Operations were uneventful, and all rabbits immediately resumed normal cage activity. In Group B, major infection was identified in one knee at 1 month after surgery and in three knees at 3 months. These infected knees were omitted from the study. As a result, nine knees at 1 month and seven knees at 3 months were assessed

**Table 1 Histological grading system[a]**

| Tissue morphology (Ti) | Intactness of calcified cartilage layer, formation of tidemark (Tide) | Lateral integration of implanted material (Latl) |
|---|---|---|
| 4 = Mostly hyaline cartilage | 1 = <25% of the calcified cartilage layer intact | 1 = Not bonded |
| 3 = Mostly fibrocartilage | 2 = 25-49% of the calcified cartilage layer intact | 2 = Bonded at one end/partially both ends |
| 2 = Mostly noncartilage | 3 = 50-75% of the calcified cartilage layer intact | 3 = Bonded at both sides |
| 1 = Exclusively noncartilage | 4 = 76-90% of the calcified cartilage layer intact | **Basal integration of implanted material (Basl)** |
| **Matrix staining (Matx)** | 5 = Complete intactness of the calcified cartilage layer | 1 = <50% |
| 1 = None | **Subchondral bone formation (Bform)** | 2 = 50-70% |
| 2 = Slight | 1 = No formation | 3 = 70-90% |
| 3 = Moderate | 2 = Slight | 4 = 91-100% |
| 4 = Strong | 3 = Strong | **Inflammation (InfH)** |
| **Structural integrity (Stru)** | **Histologic appraisal of surface architecture (SurfH)** | 1 = Strong inflammation |
| 1 = Severe disintegration | 1 = Severe fibrillation | 3 = Slight inflammation |
| 2 = Cysts or disruption | 2 = Moderate fibrillation | 5 = No inflammation |
| 3 = No organization of chondrocytes | 3 = Slight fibrillation or irregularity | **Histologic grading system (Hgtot)** |
| 4 = Beginning of columnar organization of chondrocytes | 4 = Normal | Some of the histologic variables: |
| 5 = Normal, similar to healthy mature cartilage | **Histologic appraisal defect filling (FilH)** | Tissue morphology (Ti) |
| **Chondrocytes clustering in implant (Clus)** | 1 = <25% | Matrix staining (Matx) |
| 1 = 25-100% of cells clustered | 2 = 26-50% | Structural integrity (Stru) |
| 2 = <25% of the cells clustered | 3 = 51-75% | Cluster formation (Clus) |
| 3 = No clusters | 4 = 76-90% | Tidemark opening (Tide) |
| | 5 = 91-110% | Bone formation (Bform) |
| | | Histologic surface architecture (SurfH) |
| | | Histologic degree of defect filling (FilH) |
| | | Lateral integration of defect-filling tissue (Basl) and histologic signs of inflammation (InfH) |

[a]Presentation of variables and the grading system based on a modified International Cartilage Repair Society (ICRS) grading scale [26] developed by O'Driscoll, Keeley and Salter [34].

from Group B, compared to 10 knees in controls at both 1 and 3 months.

At 1 month after surgery, defects in both Group B and the controls were filled with reparative cells. In Group B, the repair site appeared to be filled with cartilaginous tissue, which was stained with safranin O (Figures 1a and 1b). Lateral integration was well bonded at both sides of the surrounding cartilage. The surface of the repair site showed several smooth fibrous cell layers, and rounded chondrocytes formed inside the repair tissue in a convex pattern. The lower portion of the repair tissue contained hypertrophic chondrocytes that were remodeling the subchondral bone. Thus, the defects showed sequential construction of abundant inhomogeneous extracellular matrix from the surface by fibrous cells (or fibrocartilage cells), rounded chondrocytes and hypertrophic chondrocytes. Similarly, in the controls, defects consisted of inhomogeneous extracellular matrix from fibrous cells (or fibrocartilage cells), rounded chondrocytes and hypertrophic chondrocytes; however, no tendency toward uniform constitution was apparent. The defect was not filled with repaired tissue (Figures 1c and 1d). At 3 months in Group B, the repair site maintained a cartilage phenotype and was well integrated with the surrounding cartilage (Figure 2). Repaired tissue showed a columnar organization. The surface of the repair site retained a smooth and convex formation similar to the surrounding cartilage. In the controls at 3 months, the repair site had been replaced with fibrous tissue and bone (Figure 3), and in the surrounding adjacent cartilage there was evidence of osteoarthritic changes with loss of cartilage.

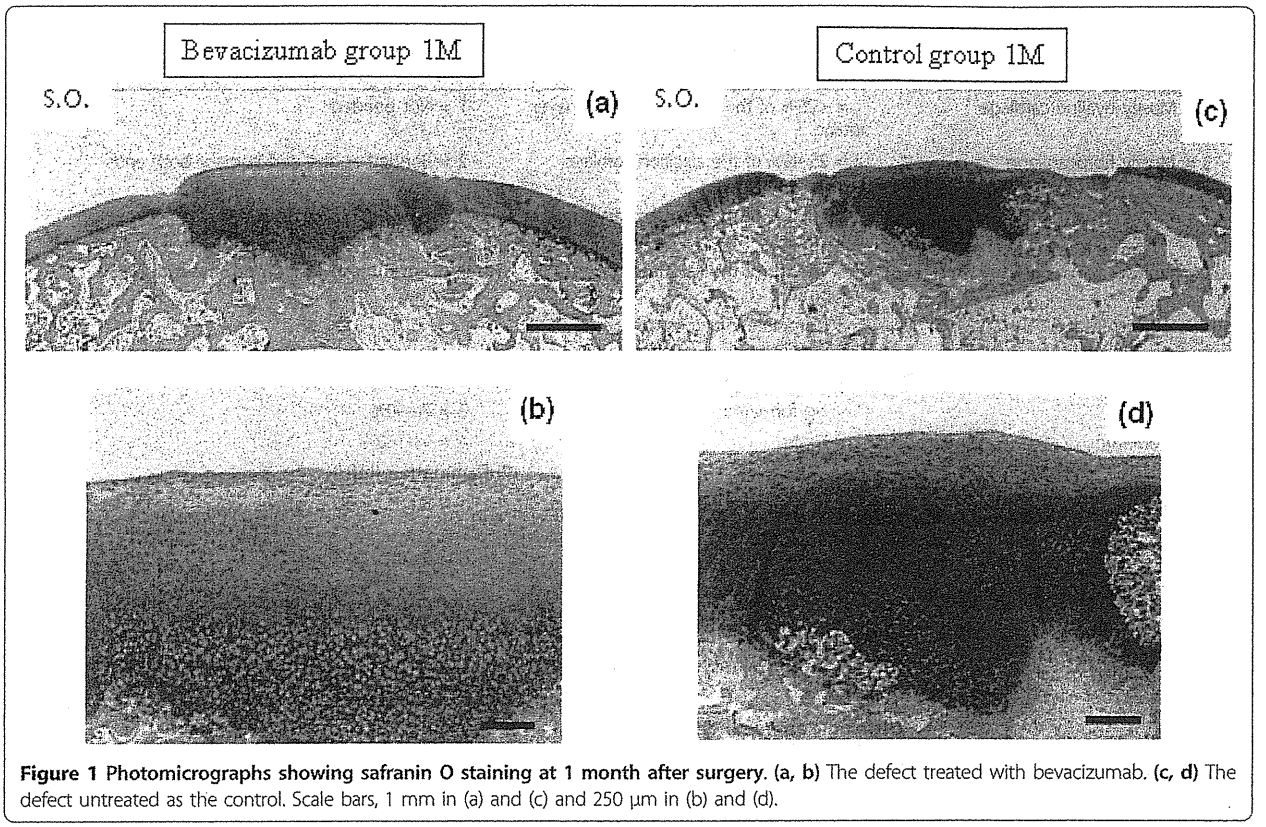


**Figure 1 Photomicrographs showing safranin O staining at 1 month after surgery. (a, b)** The defect treated with bevacizumab. **(c, d)** The defect untreated as the control. Scale bars, 1 mm in (a) and (c) and 250 μm in (b) and (d).

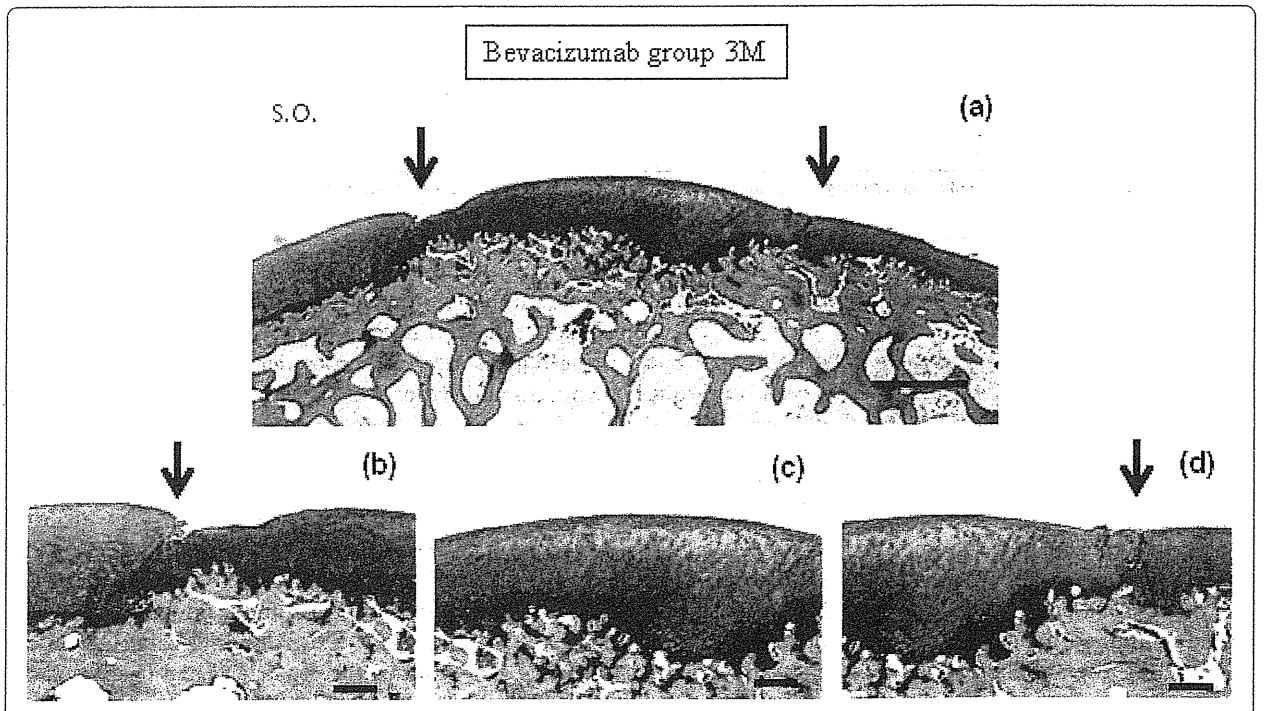


**Figure 2 Photomicrographs show safranin O staining at 3 months after surgery.** The defect was treated with bevacizumab. Bars, 1 mm in **(a)** and 250 μm in **(b, c** and **d)**.

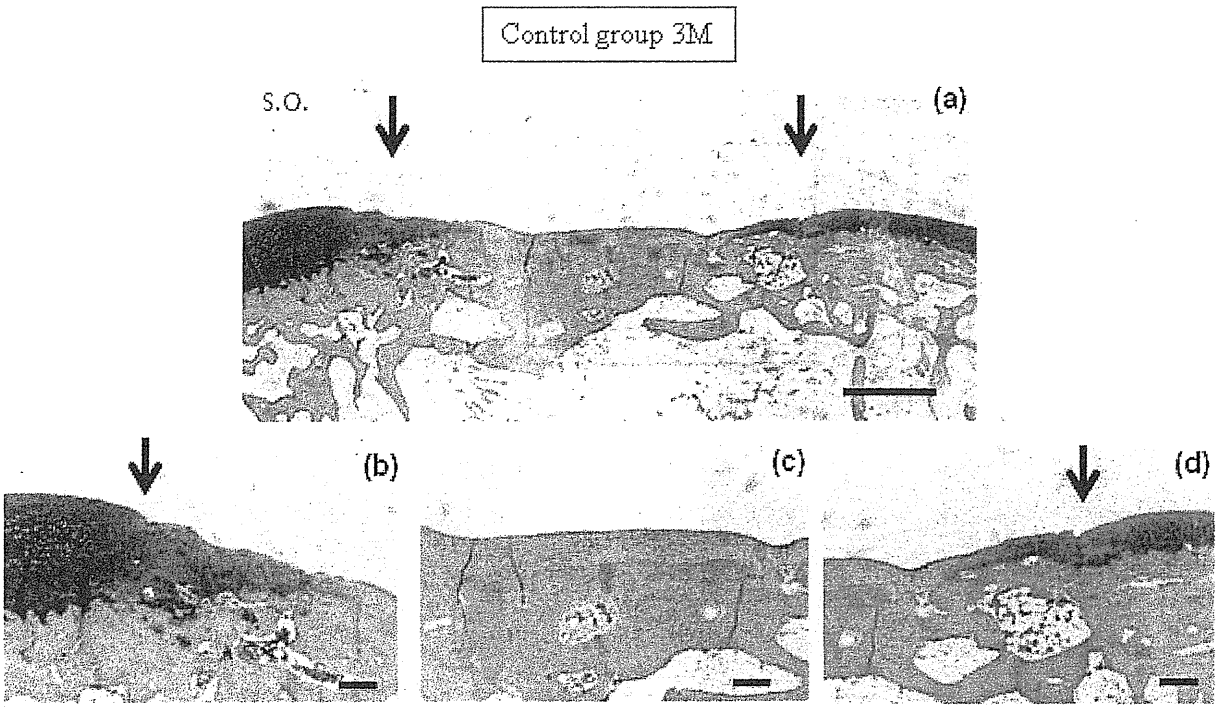


**Figure 3 Photomicrographs show safranin O staining at 3 months after surgery.** The untreated defect in the control. Bars, 1 mm in (**a**) and 250 μm in (**b, c** and **d**).

### Evaluation of ChM-I and VEGF expression

At 1 month, Group B showed intense positive results for ChM-I at the bottom of the repair tissue in the remodeling hypertrophic chondrocyte layer, representing the border between cartilage and bone (Figure 4a). ChM-I had accumulated in the interterritorial space of the repaired matrix (Figure 4a). In the controls, no ChM-I was observed in the repair tissue (Figure 4b). Conversely, the remodeling hypertrophic chondrocyte layer was intensely positive for VEGF in both Group B and in the controls (Figures 4c and 4d).

### Histological scoring of repair tissue

We evaluated the repair site using a modified version of the grading system developed by O'Driscoll, Keeley and Salter [34]. In this system, 11 histologic categories were evaluated and scored: tissue morphology (Ti), matrix staining (Matx), structural integrity (Stru), cluster formation (Clus), tidemark opening (Tide), bone formation (Bform), histologic appraisal of surface architecture (SurfH), histologic appraisal of the degree of defect filling (FilH), lateral integration of defect-filling tissue (Latl), basal integration of defect-filling tissue (Basl) and histologic signs of inflammation (InfH). The total score ranged from 11 (no repair) to 45 (normal articular cartilage) (Table 1).

At 1 month, inside the repair tissue in Group B, Ti was mostly hyaline cartilage in seven of nine cases, with high cellularity of rounded chondrocytes and mostly fibrocartilage in two of nine cases. Conversely, in the controls, 4 of 10 cases showed mostly hyaline cartilage, 4 of 10 cases were mostly fibrocartilage and 2 of 10 cases were mostly noncartilage. For Matx in Group B, six of nine cases were strong, two of nine cases were moderate and one case showed slight staining. In the controls, 5 of 10 cases were strong, 3 of 10 cases were moderate and 2 of 10 cases showed slight staining. In Group B, Stru of the defect filling revealed the beginning of columnar organization of chondrocytes in six of nine cases and no organization of chondrocytes in three of nine cases. In the controls, 3 of 10 cases showed the beginning of columnar organization, 4 of 10 cases showed no organization and 3 of 10 cases showed cysts or disruptions. In both groups, Clus was not observed except in one instance. In one instance, there was a small amount of Clus in both groups. Also, in both groups, Tide was opened in all instances. In Group B, subchondral Bform was not recognized in four of nine cases, slightly recognized in four of nine cases and strongly recognized in one of nine cases. In the control group, subchondral Bform was not recognized in 8 of 10 cases and was slightly recognized in 2 of 10 cases.

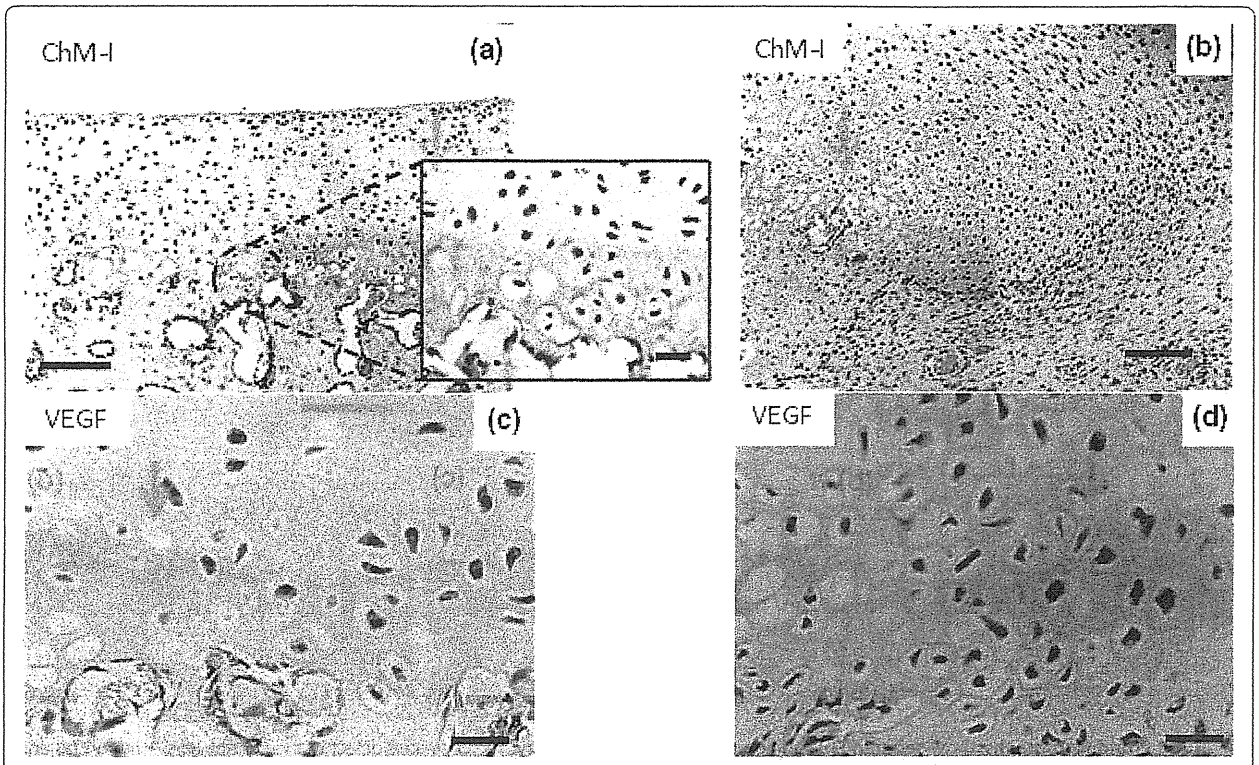


**Figure 4 Chondromodulin (ChM)-I and vascular endothelial growth factor (VEGF) localized in cartilage at 1 month after surgery. (a, c)** The defect treated with bevacizumab. **(b, d)** The defect in the control. (a) In the bevacizumab group, ChM-I immunostaining is detected in the interterritorial matrix of the remodeling site. (b) In the control group, ChM-I immunostaining is not detected in the remodeling site. (c, d) In both groups, VEGF immunostaining is detected in the remodeling site of the reparative cells. Bars, 100 μm in (a) and (b) and 25 μm in (c) and (d).

SurfH in Group B was normal in five of nine cases and showed slight fibrillation or irregularity in four of nine cases; in the control group, 1 of 10 cases was normal, 6 of 10 cases showed slight fibrillation or irregularity, 2 of 10 cases showed moderate fibrillation or irregularity and 1 of 10 cases showed severe fibrillation or disruption. FilH in Group B was complete in six of nine cases and nearly complete in three of nine cases. In controls, FilH was complete in 2 of 10 cases, nearly complete in 4 of 10 cases, moderate in 2 of 10 cases and nearly empty in 2 of 10 cases. Latl in Group B was bonded on both sides in seven of nine cases and bonded at one end or partially at both ends in two of nine cases. In controls, Latl was bonded on both sides in 1 of 10 cases, bonded at one end or partially at both ends in 6 of 10 cases and not bonded in 3 of 10 cases. Basl was good in all cases for both groups. In Group B, no inflammation was observed in all cases for InfH. The control group showed no inflammation in 5 of 10 cases, slight inflammation in 4 of 10 cases and strong inflammation in 1 of 10 cases. As a result, at 1 month, the total score was significantly higher for Group B than for the controls. In terms of individual scores, SurfH, FilH and Latl for Group B were significantly higher than in controls.

In Group B, Ti at 3 months showed mostly hyaline cartilage in six of seven cases. In one of seven cases, tissue was mostly fibrocartilage. Conversely, in the controls, 3 of 10 cases were mostly hyaline cartilage, with mostly fibrocartilage in 1 of 10 cases and exclusively noncartilage in 6 of 10 cases. For Matx, six of seven cases in Group B showed strong staining and one of seven cases showed moderate staining; in the controls, 3 of 10 cases were strong, one instance was moderate and 6 of 10 cases were nonstaining. In Group B, Stru of the defect filling revealed tissue similar to healthy mature cartilage in three of seven cases, beginning columnar organization of chondrocytes in three of seven cases and no organization of the chondrocytes in one of seven cases. In the controls, only one instance was similar to healthy mature cartilage, 2 of 10 cases were beginning columnar organization, 1 of 10 cases had no organization and 6 of 10 cases showed severe disintegration. In Group B, Clus was not observed. In controls, 2 of 10 cases showed no clusters, 2 of 10 cases showed some clusters and 6 of 10 cases showed abundant cluster cells or nonchondrocytes. Tide in Group B was complete in three of seven cases, nearly complete in two of seven cases, half degree in one of seven cases and nearly

absent in one of seven cases; in the controls, 1 of 10 cases was complete, 2 of 10 cases were nearly complete, 1 of 10 cases was half degree and 6 of 10 cases were not recognized as containing a calcified cartilage layer. Bform was recognized in both groups, except for one instance in each. In one instance, there was a slightly Bform in both groups. SurfH in Group B was normal in five of seven cases and showed slight fibrillation or irregularity in two of seven cases; in the controls, 1 of 10 cases was normal, 1 of 10 cases showed slight fibrillation or irregularity, 2 of 10 cases showed moderate fibrillation or irregularity and 6 of 10 cases showed severe fibrillation or disruption. FilH in Group B was complete in all instances. In the controls, FilH was complete in 4 of 10 cases, moderate in 1 of 10 cases, nearly empty in 1 of 10 cases and almost empty in 4 of 10 cases. Latl in Group B were bonded at both sides in six of seven cases and bonded at one end in one of seven cases. In the controls, Latl was bonded both sides in 1 of 10 cases, bonded at one end or partially both ends in 2 of 10 cases and not bonded in 6 of 10 cases. Basl was good in all cases in both groups. For InfH, no inflammation was observed in any cases in either group. At 3 months, the total score for Group B was significantly higher than that for the controls. In terms of individual scores, Ti, Matx, Stru, Clus, SurfH, FilH and Latl were significantly higher for Group B than for the control group (Table 2).

## Discussion

VEGF is overexpressed in numerous solid angiogenic tumors and hematological malignancies. Interrupting the VEGF pathway has thus become a major focus of oncology research [35]. The first approved antiangiogenic therapy was bevacizumab, a humanized monoclonal anti-VEGF antibody. Following the success of a pivotal trial, the FDA approved bevacizumab for use in combination with intravenous 5-fluorouracil-based chemotherapy as a treatment for patients with first-line or previously untreated metastatic cancer of the colon or rectum [36]. Bevacizumab is anticipated to be useful not only for cancer treatment but also as a major advance in antiangiogenic therapy.

**Table 2 Histological scores for cartilage repair at 1 month and 3 months after surgery[a]**

| | 1 month | | 3 months | |
|---|---|---|---|---|
| | Group B | Control | Group B | Control |
| Ti | 3.77 ± 0.4 | 3.20 ± 0.7 | 3.85 ± 0.3* | 2.10 ± 1.4 |
| Matx | 3.55 ± 0.7 | 3.30 ± 0.8 | 3.71 ± 0.7* | 2.10 ± 1.4 |
| Stru | 3.66 ± 0.5 | 3.00 ± 0.8 | 4.28 ± 0.7* | 2.41 ± 1.6 |
| Clus | 2.88 ± 0.3 | 2.90 ± 0.3 | 3.00 ± 0.0* | 1.60 ± 0.8 |
| Tide | 1.00 ± 0.0 | 1.00 ± 0.0 | 3.85 ± 1.4 | 2.20 ± 1.6 |
| Bform | 1.66 ± 0.7 | 1.20 ± 0.4 | 2.85 ± 0.3 | 2.90 ± 0.3 |
| SurfH | 3.55 ± 0.5* | 2.70 ± 0.8 | 3.71 ± 0.4* | 1.70 ± 1.0 |
| FilH | 4.66 ± 0.5* | 3.70 ± 1.0 | 5.00 ± 0.0* | 2.90 ± 1.9 |
| Latl | 2.77 ± 0.4* | 1.80 ± 0.6 | 2.85 ± 0.3* | 1.60 ± 0.8 |
| Basl | 4.00 ± 0.0 | 4.00 ± 0.0 | 4.00 ± 0.0 | 4.00 ± 0.0 |
| InfH | 5.00 ± 0.0 | 3.80 ± 1.3 | 5.00 ± 0.0 | 5.00 ± 0.0 |
| Hgtot | 36.55 ± 2.1* | 30.50 ± 4.1 | 40.14 ± 2.5* | 27.7 ± 10.0 |

[a]Values are means ± SD. The total score range is from 11 (no repair) to 45 (normal articular cartilage).

*Denotes significance at $P < 0.05$.

Generally, osteochondral defects have access to reparative cells of the bone marrow [37]. This connection allows infiltration of the bone by mesenchymal stem cells (MSCs) from the bone marrow, which can then proliferate and differentiate. MSC-derived chondrocytes subsequently appear during endochondral ossification and are invaded by the vasculature and marrow, and eventually the defects are replaced by subchondral bone [28,38]. In summary, MSC-derived chondrocytes are spontaneously recruited as reparative cells in osteochondral defects and are replaced by bone with high levels of vascular invasion. However, articular cartilage is a naturally avascular tissue, except during skeletal development, when endochondral bone formation occurs. We speculate that MSCs may use different courses of differentiation to become bone or cartilage, based on environmental differences in vascularization and avascularization. We recently reported that MSCs that acquire antiangiogenic properties achieve good cartilage restoration [23]. Furthermore, previous research has shown that VEGF expression by chondrocytes in osteoarthritic joints may be related to articular cartilage destruction [39-46]. High-dose VEGF may induce the onset and progression of arthritis [47,48]. Also, expression of high levels of VEGF during the terminal stages of chondrogenesis leads to endochondral ossification through angiogenesis [49,50]. We therefore studied the restoration of articular cartilage by blocking VEGF signaling with bevacizumab in a model of osteochondral defects in Japanese white rabbits.

At 1 month after surgery in both Group B and the controls, defects were recruited with reparative cells from the marrow and synovial tissue, and this was composed of differentiated chondrocytes, hyperchondrocytes and fibrous cells. These heterogeneous cells stained positive for safranin O and showed various levels of structured organization. From the surface, these structures consisted of a fibrous or fibrocartilage layer, a hyaline cartilage layer and a hypertrophic chondrocyte layer in both groups. As a result, no significant differences were apparent between the two groups at 1 month postoperatively in Ti, Matx or Stru. However, at 1 month after surgery, the defects were repaired by hyaline cartilage (seven of nine cases) in Group B, a result of blocking VEGF, whereas in the controls, the defects were repaired with that of various tissues, including hyaline

cartilage (4 of 10 cases), fibrocartilage (4 of 10 cases) and noncartilage (2 of 10 cases). There was no delay in subchondral bone formation in Group B when blocking VEGF. For autologous reparative cells, basal integration was good and most inflammatory signs were absent from both groups. On the other hand, FilH, Latl and SurfH were significantly higher for Group B than for the controls. Actually, at 1 month after surgery, six of nine cases in Group B showed convex surfaces of these repaired tissues in surrounding articular cartilage, compared to only 2 of 10 cases in the controls. These results indicate that blocking VEGF preserves the accumulation of reparative cells in the defect. This is supported by studies showing that VEGF treatment prevents condensation of chondrogenic mesenchyme during early limb bud development through abnormal vascularization [51]. As a sufficient number of reparative cells made contact with the surrounding cartilage layer, lateral integration was considered to be good. Also, repaired tissue taking a convex form consisted of a smoother surface than repaired tissue with a concave form.

Defects had been repaired by the formation of various tissues in the controls at 3 months after surgery, which included hyaline cartilage (3 of 10 cases), fibrocartilage (1 of 10 cases) and exclusively noncartilage (6 of 10 cases). On the other hand, when blocking VEGF, defects were repaired mostly with hyaline cartilage (six of seven cases), with only one case being mostly fibrocartilage. To emphasize this, no cases showed replacement by fibrous tissue or bone. Similarly, 1 month after surgery, the controls showed repair without consistent tissue morphology, while Group B showed repair with consistency of tissue morphology. At 3 months postoperatively, Ti, Matx, Stru and Clus were significantly higher for Group B than for the controls. In both Group B and the controls, Tide was generally closed and bone formation was gradually observed. Continuous basal integration was also good and most signs of inflammation were not apparent in either group. Tissue that was repaired in the form of fibrous tissue and bone tended to show moderate or severe fibrillation of surface architecture and low defect filling. Therefore, SurfH and FilH were significantly higher for Group B than for the controls. As mentioned before, a sufficient number of reparative cells were in contact with the surrounding cartilage layer, and lateral integration was considered to be good. As a result, at 3 months, the total score was significantly higher for Group B than for the controls.

Interestingly, ChM-I was expressed in the early stage of tissue repair after bevacizumab administration. ChM-I reportedly stimulates chondrocyte proliferation and proteoglycan synthesis in vitro and inhibits proliferation of vascular endothelial cells in vitro and in vivo [52,53]. Kitahara *et al.* [53] suggested that in their mouse model, ChM-I acts to inhibit vascular invasion in the immature state of articular cartilage, and levels of ChM-I gradually decrease with age thereafter. Hiraki *et al.* [52] reported that ChM-I is expressed in the avascular zone of cartilage in developing bone, but is not present in calcifying cartilage. Such findings suggest a regulatory role of ChM-I in vascular invasion during endochondral bone formation.

In this study, ChM-I was expressed at the bottom of the repair site invaded near the vasculature. ChM-I accumulated in the interterritorial space of the repaired matrix and was surrounding the cells that expressed VEGF. ChM-I is thought to form a barrier to inhibit vascular invasion from subchondral bone, indicating that it facilitates the acquisition of articular cartilage through the process of MSC differentiation in endochondral ossification. However, the shift from angiogenesis to antiangiogenesis is not determined entirely by ChM-I and VEGF. Inducers of endogenous angiogenic molecules also exist in the process of endochondral ossification, and these include VEGF [53], fibroblast growth factor 2 [54], transforming growth factor [55] and tissue matrix metalloprotease 9 [56].

In other studies, VEGF has been reported to be necessary for chondrocyte survival during cartilage development. In VEGF-deficient mouse models, massive cell death is observed in the joint and epiphyseal regions of cartilage during cartilage development [57,58]. In this study, we blocked VEGF temporarily to initiate reparative cells. To avoid complete inhibition of the bioactivity of VEGF in reparative cells, we blocked VEGF on the day of surgery and 2 weeks later. As a result, 1 month after surgery, reparative cells actually expressed VEGF in Group B (Figure 4c). Moreover, expression of ChM-I as an antiangiogenic factor was observed in the layer of reparative cells involved in blood vessel invasion from subchondral bone (Figure 4a). It is important to consider the efficacy of various VEGF treatments in the balance of angiogenesis-antiangiogenesis during chondrogenic differentiation of MSC-derived reparative cells. In other words, repair of articular cartilage may be achievable by adjusting optimal VEGF signaling. In a recent study, Kubo *et al.* [39] reported good cartilage restoration using muscle-derived stem cells that transfected with the genes of Flt-1 (a VEGF antagonist) and bone morphogenetic protein (BMP) 4 in a mouse osteochondral defect model. However, the techniques applied in that study were complicated, as they required isolation of stem cells from muscular tissue, gene transduction and cell culture in vitro, as well as cell transplantation. Conversely, the present technique involves the simple means of achieving cartilage restoration by intravenous administration of bevacizumab, a treatment already cleared for clinical application. Hence,

this method would be applicable in many medical facilities. Thus, vascularization of the tissue environment after injury or degeneration would be improved to a more advantageous situation of cartilage repair if VEGF were blocked. Accordingly, without depending on cells or tissue transplantation, this approach would augment the curative effects of existing approaches such as microfracture or drilling.

The half-life of bevacizumab in the circulation of humans is reportedly 17-21 days. The approved dose of bevacizumab in humans is 5 mg/kg, and the clinical administration interval is more than 2 weeks [30]. Bevacizumab is cross-reactive with rabbit VEGF, but has eightfold lower affinity for rabbit VEGF than for human VEGF [59]. Therefore, in this study, we investigated bevacizumab at the dose of 40 mg/kg administered on the day of surgery and 2 weeks later. As a future consideration, we plan to investigate the dosage and duration of bevacizumab administration. We will also address the side effects of infection by applying minimally invasive surgery with an arthroscope and using antibiotics.

## Conclusions

Temporary intravenous administration of the humanized monoclonal anti-VEGF antibody bevacizumab in an osteochondral defect model results in positive restorative effects. We suggest that this approach would be useful to achieve repair of articular cartilage without the need for cells or tissue transplantation.

### Abbreviations

BASL: basal integration of defect-filling tissue; BFORM: bone formation; BMP: bone morphogenetic protein; BSA: bovine serum albumin; CHM-I: chondromodulin-I; CLUS: cluster formation; EDTA: ethylenediaminetetraacetic acid; FILH: histologic appraisal of the degree of defect filling; ICRS: International Cartilage Repair Society; INFH: histologic signs of inflammation; LATL: lateral integration of defect-filling tissue; MATX: matrix staining; PBS: phosphate-buffered saline; SD: standard deviation; STRU: structural integrity; SURFH: histologic appraisal of surface architecture; TI: tissue morphology; TIDE: tidemark opening; VEGF: vascular endothelial growth factor.

### Acknowledgements

This research was partly supported by Grants-In-Aid for Scientific Research from the Ministry of Education, Culture, Sports, Science and Technology of Japan, and Mitsui Sumitomo Insurance Welfare Foundation.

### Authors' contributions

TN and MS performed most of the experiments and MK performed the immunohistochemistry. TK, GE and NO helped with in vivo experiments. TN performed statistical analyses. MS and JM designed and coordinated the study and helped draft the manuscript. All authors approved the final manuscript.

### Competing interests

The authors declare that they applied for a patent relating to the content of the manuscript in Japan, but did not receive any reimbursements, fees, funding or salary from an organization. The competitive companies developing or selling anti-VEGF drugs (e.g., Novartis, Wyeth, Bayer Schering) may keep them in check.

Received: 17 May 2010 Revised: 31 July 2010
Accepted: 24 September 2010 Published: 24 September 2010

### References

1. Paget J: Healing of cartilage. *Clin Orthop Relat Res* 1969, 64:7-8.
2. Pridie KH: A method of resurfacing osteoarthritic knee joints. *J Bone Joint Surg Br* 1959, 41:618-619.
3. Muller B, Kohn D: Indication for and performance of articular cartilage drilling using the Pridie method. *Orthopade* 1999, 28:4-10.
4. Insall JN: Intra-articular surgery for degenerative arthritis of the knee. A report of the work of the late K. H. Pridie. *J Bone Joint Surg Br* 1967, 49:211-228.
5. Insall J: The Pridie debridement operation for osteoarthritis of the knee. *Clin Orthop* 1974, 101:61-67.
6. Steadman J, Rodkey W, Briggs K, Rodrigo J: The microfracture technique in the management of complete cartilage defects in the knee joint. *Orthopade* 1999, 28:26-32.
7. Steadman J, Rodkey W, Rodrigo J: Microfracture: surgical technique and rehabilitation to treat chondral defects. *Clin Orthop Relat Res* 2001., 391 Suppl: S362-S369.
8. Steadman J, Rodkey W, Briggs K: Microfracture to treat full-thickness chondral defects: surgical technique, rehabilitation, and outcomes. *J Knee Surg* 2002, 15:170-176.
9. Mithoefer K, Williams RJ, Warren RF, Potter HG, Spock CR, Jones EC, Wickiewicz TL, Marx RG: Chondral resurfacing of articular cartilage defects in the knee with the microfracture technique: surgical technique. *J Bone Joint Surg Am* 2006, 88:294-304.
10. Hangody L, Kish G, Karpati Z, Udvarhelyi I, Szerb I, Bely M: Autogenous osteochondral graft technique for replacing knee cartilage defects in dogs. *Orthopedics* 1997, 5:175-181.
11. Hangody L, Feczko P, Bartha L, Bodo G, Kish G: Mosaicplasty for the treatment of articular defects of the knee and ankle. *Clin Orthop Relat Res* 2001, , 391 Suppl: S328-S336.
12. Szerb I, Hangody L, Duska Z, Kaposi NP: Mosaicplasty: long-term follow-up. *Bull Hosp Jt Dis* 2005, 63:54-62.
13. Brittberg M, Lindahl A, Nilsson A, Ohlsson C, Isaksson O, Peterson L: Treatment of deep cartilage defects knee with autologus chondrocyte transplantation. *N Engl J Med* 1994, 331:889-895.
14. Peterson L, Minas T, Brittberg M, Lindahl A: Treatment of osteochondritis dissecans of the knee with autologouschondrocyte transplantation: results at two to ten years. *J Bone Joint Surg Am* 2003, 85-A Suppl 2:17-24.
15. Zaslav K, Cole B, Brewster R, DeBerardino T, Farr J, Fowler P, Nissen C, STAR Study Principal Investigators: A prospective study of autologous chondrocyte implantation in patients with failed prior treatment for articular cartilage defects of the knee: results of the Study of the Treatment of Articular Repair (STAR) clinical trial. *Am J Sports Med* 2009, 37:42-55.
16. Moseley JB Jr, Anderson AF, Browne JE, Mandelbaum BR, Micheli LJ, Fu F, Erggelet C: Long-term durability of autologus chondrocyte implantation: a multicenter, observational study in US patients. *Am J Sports Med* 2010, 38:238-46.
17. Darling EM, Athanasiou KA: Articular cartilage bioreactor and bioprocess. *Tissue Eng* 2003, 9:9-26.
18. Backwalter JA, Lohmander S: Operative treatment of osteoarthrosis. Current practice and future development. *J Bone Joint Surg Am* 1994, 76:1405-1418.
19. Freed LE, Grande DA, Lingbin Z, Emmanual J, Marquis JC, Langer R: Joint resurfacing using allograft chondrocytes and synthetic biodegradable polymer scaffolds. *J Biomed Mater Res* 1994, 28:891-899.
20. Hunziker EB: Articular cartilage repair: basic science and clinical progress. A review of the current status and prospects. *Osteoarthritis Cartilage* 2002, 10:432-463.
21. Marcacci M, Berruto M, Brocchetta D, Delcogliano A, Ghinelli D, Gobbi A, Kon E, Pederzini L, Rosa D, Sacchetti GL, Stefani G, Zanasi S: Articular cartilage engineering with Hyalograft C: 3-year clinical results. *Clin Orthop Relat Res* 2005, 435:96-105.
22. Crawford DC, Heveran CM, Cannon WD Jr, Foo LF, Potter HG: An autologus cartilage tissue implant NeoCart for treatment of grade III chondral injury to the distal femur: prospective clinical safety trial at 2 years. *Am J Sports Med* 2009, 37:1334-1343.